Testing approaches and sensors for satellite-derived bathymetry in Nunavut

Kiyomi Holman

Thesis submitted to the University of Ottawa in partial Fulfillment of the requirements for the degree of Master of Science in Geography

Department of Geography, Environment, and Geomatics
Faculty of Arts
University of Ottawa

Supervisor:
Dr. Anders Knudby

Thesis Committee:
Dr. Luke Copland
Dr. Michael Sawada

Abstract

Nearshore bathymetry in the Canadian Arctic is poorly surveyed, but is vital knowledge for coastal communities that rely on marine transportation for resources and development. Nautical charts currently available are often outdated and surveying by traditional methods is both time consuming and expensive. Satellite-derived bathymetry (SDB) offers a significantly cheaper and faster option to provide information on nearshore bathymetry. The two most common approaches to SDB are empirical and physics-based. The empirical approach is simple and typically does well when calibrated with high-quality in-situ data, whereas the physics-based approach is more difficult to implement and requires precise atmospheric correction. This project tests the practical use of five methods within the empirical and physics-based approaches to SDB, using Landsat 8 and Sentinel-2 satellite imagery, at seven sites across Nunavut. Methods tested include: the Ratio-Transform, Multiband, and Random Forest Regression methods (empirical) and radiative transfer modeling (physics-based) using two atmospheric correction models: ACOLITE and Deep Water Correction. All methods typically use geolocated water depth data for validation, as well as calibration for the empirical methods. Spectral reflectance for model inputs were collected in Cambridge Bay, NU. Water depth data were acquired from the Canadian Hydrographic Service. All processing was conducted within the framework of plugins developed for the open-source GIS software, QGIS. Results from the empirical methods were typically poor due to poor calibration data, though Random Forest Regression performed well when good calibration data were available. Due to poor quality validation data, error for the physics-based results cannot be adequately quantified in most places. Additionally, atmospheric correction remains a challenge for the physics-based methods. Overall, results indicate that where large, high-quality calibration datasets are available, Random Forest Regression performs best of all methods tested, with little bias and low mean absolute error in water less than 10 m deep. As such datasets are rare in the Arctic, the physics-based method is often the only option for SDB and is an excellent qualitative tool for informing communities of shallow bathymetry features and assessing navigation risk.

Acknowledgements

For all his patience, guidance, support, and the opportunities I am grateful to have had because of him, I'd like to thank Dr. Anders Knudby. Despite being an atypical student, he has been understanding and unwavering in his support through my journey to complete this project. I am so honoured to have been your student. Now that I am finished perhaps you and Kevin can finally have that Civ match. Just go easy on him.

Thank you to my thesis committee members, Dr. Luke Copland and Dr. Michael Sawada, for providing excellent feedback and support. I would also like to thank those with the Nunavut General Monitoring Plan, the Northern Scientific Training Program, and Natural Resources Canada for their support and providing the funding for this research, as well as DigitalGlobe Foundation and the Canadian Hydrographic Service for providing data.

Additional thanks must be extended to the many people we worked with in Cambridge Bay: POLAR Knowledge Canada for their hospitality and logistical assistance, the Cambridge Bay Fire Department for the oxygen tank fills, Chris Arko for being the most "HARDKOR" Arctic dive partner a newbie could have asked for, Angulalik Pedersen for his assistance in all things Cambridge Bay, and finally Gerry Chidley and the boys of the R/V Martin Bergmann for more oxygen fills, as well as lending us a boat and Darcy for data collection. Because of all this help, our field work was a great success and immensely enjoyable.

I must also thank Alexander Tamm for his extensive help and being my 'rubber ducky' when working through programming problems. He was an invaluable part of my learning during the last portion of my program.

Lastly, I would like to thank my friends, family, and most especially my husband Kevin, for their love and continued faith in me and my abilities during my research. The climbing trips, family meals in Ottawa or at home, and countless pep talks were always there precisely when I needed them most. Cheers.

Table of Contents

List of Figures

List of Tables

Chapter 1

Introduction

Coastal communities rely on maritime transportation for development and supplies. Knowledge of nearshore bathymetry, which is vital for safety of navigation, is thus crucial for any coastal nation. While many resources for safe travel are typically made available to mariners via nautical charts and positioning in relation to shoreline or seamarks, accurate data on bathymetry is limited in dynamic and poorly charted environments such as the Canadian Arctic. Decreasing sea ice cover and increasing vessel traffic has added pressure to the need for accurate bathymetric information, but up-to-date charts are rarely available (Anisimov et al., 2007; Chénier et al., 2018). Information on bathymetry in the Canadian Arctic remains extremely inadequate, with only 1% of the Arctic surveyed to modern standards (Leach et al., 2014). Water depth data that does exist is either concentrated on small areas of importance such as harbours, is out-dated (either by actual date surveyed, or by methods used), or is non-existent with no prospects of being surveyed due to high cost and challenging environmental hazards (Chénier et al., 2018).

Most bathymetric data are collected via ship-borne multibeam echo soundings (MBES) or single-beam echo soundings (SBES), or using Airborne Lidar Bathymetry (ALB). While these methods produce high quality data, surveying is both expensive and extremely time consuming. Due to such challenges, researchers have focused on developing and improving cheaper methods of deriving bathymetry since the late 1970's. Satellite-derived bathymetry (SDB) may produce a broader base of knowledge from which to inform marine traffic, responsible environmental practises and, depending on the approaches used, can produce information on water quality and coastal habitats which can be utilised for environmental monitoring. Four approaches are typically used in SDB: 1) Empirical approaches, which utilize *in situ* georeferenced water depth data to establish a statistical relationship between water depth and pixel colour and then estimates bathymetry based on extrapolation of that relationship (Lyzenga, 1978, 1985; Stumpf et al. 2003); 2) Physics-based approaches, which use radiative transfer modeling (RTM) to predict ocean colour as a function of water quality, depth and seafloor reflectance, and then invert the model by matching the observed colour of each pixel to the modeled ocean colour it most closely resembles (Knudby et al. 2016; Lee et al. 1998, 1999); 3) Photogrammetry, which utilizes stereo imagery to estimate bathymetry based on geometric relationships (Hodúl et al.,

2020); and 4) Wave Kinematic Bathymetry, which relies on a dispersion equation to relate the celerity of ocean waves to water depth (Poupardin et al. 2016).

While these four categories, and many of the specific methods within each one, are themselves well-established, their relative performance in different environments is not well established and likely depends on factors such as image quality and environmental conditions as well as the availability of ancillary data. In this thesis, empirical and physics-based SDB approaches are explored for areas around seven coastal communities in the Canadian Arctic. In addition, work for this thesis also produced a series of plugins for the open source GIS software QGIS, which will allow non-experts to conduct their own SDB analysis. This is of particular importance to communities in which access to resources for surveying is limited, such as in the Canadian Arctic.

1.1 Thesis Objective

The main objective of this thesis is to test and compare the possibility of using three empirical methods and the physics-based approach for SDB in the shallow marine environments around seven coastal communities in Nunavut, Canada, given currently available data. Tested satellite sensors include Landsat-8 OLI and Sentinel-2 MSI. In combination, this thesis will provide information to improve understanding of the accuracies that can be expected from different SDB approaches, for different parts of the Arctic, with different satellite sensors. This objective will be accomplished by producing a series of plugins with Graphical User Interfaces (GUIs) to perform SDB analysis within the QGIS environment.

1.2 Thesis Format

This thesis presents the paper “Testing approaches and sensors for satellite-derived bathymetry in the Canadian Arctic” in Chapter 2 with the intention to submit for publication. Conclusions and references are presented as Chapters 3 and 4 respectively, followed by two Appendices containing the complete results from the project, and a user manual for the QGIS plugin discussed in Chapter 2.

Chapter 2

Testing Approaches and Sensors for SDB in the Canadian Arctic

2.1 Introduction

Knowledge of nearshore bathymetry and safe shipping routes are vital to coastal communities that depend on marine transportation for development and resources. In the Arctic, where many communities are coastal and increases in nearshore activity are projected as melting sea ice uncovers new potential shipping routes, such knowledge is critically important (Leach et al., 2014). However, bathymetric surveys of shallow waters (< 20 metres) in the Arctic happen slowly due to the hazardous and remote environment, limited resources, and high costs to complete surveys with traditional methods such as airborne lidar or ship-based acoustic sounding (Chénier et al., 2018). Ongoing developments in the field of satellite-derived bathymetry (SDB) provide an alternative to the current practises, mapping bathymetry for the region's shallow waters using technology that is significantly more efficient than acoustic sounding methods both with respect to time and cost.

SDB estimates water depth based on satellite data depicting ocean colour. Observation of the sea floor in satellite imagery is limited by water clarity, but can be used to derive bathymetry in optically shallow waters – where sunlight reflecting off the seafloor has a detectable influence on the colour of an area as seen from space (Knudby et al. 2016). Accuracy in water depth estimation is affected by variables such as seafloor reflectance, sun-sensor geometry, sun glint, wind, and the optical properties of the water (Knudby et al., 2016). To date, several SDB approaches have been tested and can be broadly categorized by their methodologies: empirical, physics-based, photogrammetric, and wave-kinematic (Lyzenga, 1978, 1985; Stumpf et al., 2003; Lee et al., 1998, 1999; Hodúl et al., 2020; Poupardin et al., 2016).

All methods typically make use of geolocated water depth information for validation, and the empirical methods also require such data for calibration. This poses a significant challenge as very little of the Canadian Arctic has been surveyed to modern standards. Of the surveys that have been done, many used methods that are now considered outdated (e.g. lead-lining, geolocation by compass-triangulation), and others may be out of date due to morphological changes from sediment transport, deposition, and erosion (Chénier et al. 2019) – some current

charts of Canadian waters are based on data that, at the time of writing, were collected more than 200 years ago (e.g. Charts 5135 and 5138 of Greep Point, NL).

As a response to the urgent need for updated knowledge of nearshore areas, this project seeks to test the feasibility of using variations of the empirical and physics-based approaches as they are currently used across seven sites in Nunavut, Canada, and determine the relative performance of different sensors and methods at each site. A GUI-based plugin was developed for the open-source software QGIS to perform the SDB analysis. This plugin will be made available in the QGIS plugin repository for public use under the name "SDB Tools". It is intended that the information derived from the data products of the plugin can assist Northern communities in decision-making processes to which knowledge of shallow-water bathymetry can contribute.

2.2 Study Sites

The seven largest coastal communities in Nunavut were selected for this study (Figure 1). All are impacted by seasonal ice cover and nearby river outflows, and the seven sites represent a range in latitude as well as their physical characteristics such as turbidity, tidal range, and average water depth. There is at least one site situated within each of the five marine domains of the Canadian Arctic (Oceans North Conservation Society et al., 2018), apart from the High Arctic:

1. Kugluktuk (67.8° N, 115.1° W) - Located within the Beaufort-Amundsen domain, within Coronation Gulf on the delta of the Coppermine River in southwestern Nunavut. The physical characteristics of the marine environment are dominated by Arctic Ocean waters, have seasonal ice cover, and outside Coronation Gulf waters are bounded by sills to the north and east (Melling, 2002). Tidal stage changes very little, fluctuating by ~ 0.3 m (DFO, 2020). It is also within the Kazan region of the Canadian Shield, an area characterized by vast plateaus and lowlands as well as broad, sloping uplands (Natural Resources Canada, 2020).

2. Cambridge Bay (69.1° N, 105.1° W) - Located on southern Victoria Island within the Kitikmeot domain. The bay itself is narrow and deep, and is characterised by seasonal ice cover, Arctic surface waters, with sills to the north, west and east. Tidal fluctuations are typically < 1 m (DFO, 2020). It is part of the Arctic Lowlands with extensive regions of

flat topography (Natural Resources Canada, 2020). Visibility in the waters of Cambridge Bay is high.

3. Arviat (61.1° N, 94.1° W) - Located within the Hudson-Foxe domain, on the western rim of Hudson's Bay, south of Rankin Inlet. Water near Arviat has seasonal ice cover and is dominated by Arctic surface waters. Tidal fluctuations range between roughly 0 – 4 m (DFO, 2020). The region is bounded by a shallow sill to the northwest. Located within the Kazan region of the Canadian Shield as well.

4. Rankin Inlet (62.8°N, 92.1° W) – Located within the Hudson-Foxe domain, north of Arviat, and shares similar characteristics though tidal influences are slightly stronger, ranging between 0 – 4.5 m typically (DFO, 2020).

5. Igloolik (69.4° N, 81.8° W) - Located in the Hudson-Foxe domain, on a small island northwest of Prince Charles Island. Also has seasonal ice cover and is dominated by Arctic surface waters. Tides range between 0 – 3 m (DFO, 2020). The region is bounded by a shallow sill to the northwest Within the Foxe Plain region of Arctic Lands, it is characterised by regions of vast flat topography (Natural Resources Canada, 2020). Waters near Igloolik are very deep, but clear.

6. Pond Inlet (72.7° N, 78.0° W) - Located at the northern side of Baffin Island within the Baffin-Labrador marine domain, it is the northernmost of all study site locations. It experiences seasonal ice cover, is dominated by Arctic surface waters, and is bounded by shallow sills to the north, south, and west. Water clarity is poor due to the influence of the adjacent river. It is within the Davis region of the Arctic Lands. This area is characterised by high surface relief, though Pond Inlet itself is on a river delta. At the time when preprocessing and processing work for this project was conducted, no tidal stage data were available.

7. Iqaluit (63.7° N, 68.5° W) - On the southeastern side of Baffin Island within Frobisher Bay, Iqaluit has seasonal ice cover, and is dominated by Arctic surface waters. Iqaluit

experiences very large tidal fluctuations up to 11.5 m (DFO, 2020). Situated on the Everett Mountains within the Arctic Cordillera with typical glacial topography, the relief in the region is generally high and old erosion surfaces mark the landscape (Natural Resources Canada, 2020).

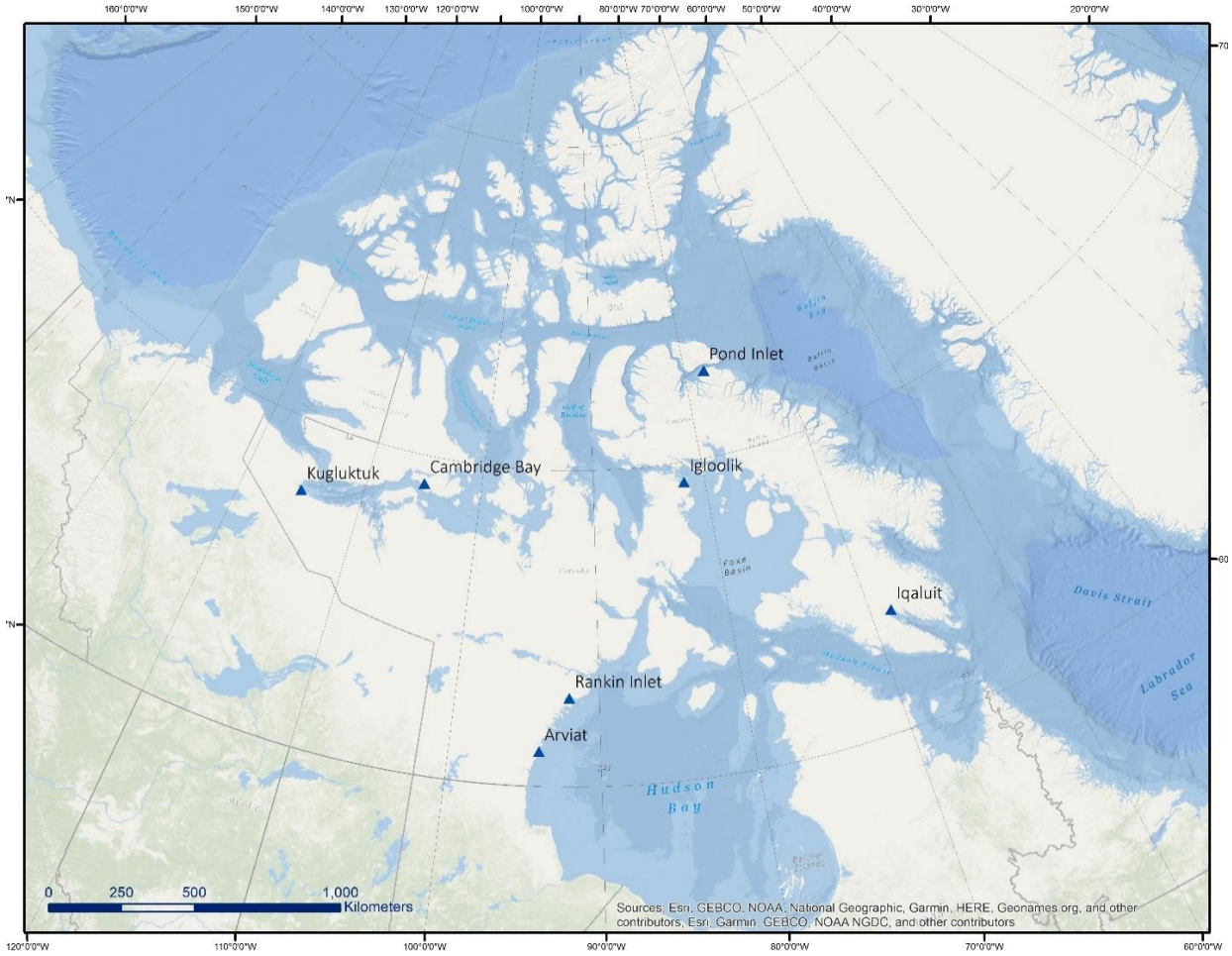

Figure 1 – Study sites.

2.3 Data

In addition to satellite imagery, this project required seafloor reflectance data for the physics-based approach, and geolocated water depth data for the empirical approach and for validation of each method.

2.3.1 Satellite Imagery

The satellite sensors Landsat 8 OLI and Sentinel-2A/B MSI were used for the project (Table 1). At the time of data acquisition and processing, the image archive that existed for Sentinel-2 was limited at each study site, affecting results. Additionally, it was found that the river adjacent to Pond Inlet produces a large and consistent sediment plume in the ice-free season, rendering the water optically deep even very close to shore, and thus unsuitable for SDB. Finding imagery at Pond Inlet that was both ice- and cloud- free, and was acquired at a low solar zenith angle, also proved to be challenging due to its high latitude. For these and other reasons detailed further on, Pond Inlet was removed from the study. Imagery for all remaining sites was reviewed during ice-free months (typically July-September) from 2016 to 2019, with the best image from each sensor selected based on visual interpretation (Table 2).

Table 1 – Technical specifications for sensors used in this project.

	Landsat 8 OLI	**Sentinel-2A&B MSI**
Bands Used	1 – 4, 5	1 – 4, 8
Spatial resolution	30 m	1 @ 60 m, 2 – 4 & 8 @ 10 m
Image extent	180 x 185 km²	100 x 100 km²
Repeat frequency	16 days	5 days
Data policy	Free	Free

Table 2 – Image acquisition dates and time (Greenwich Mean Time) for all study sites.

Study Site	**Landsat 8 Acquisition Date**	**Acquisition Time (GMT)**	**Sentinel-2 Acquisition Date**	**Acquisition Time (GMT)**
Kugluktuk	19 July, 2017	19:08:05	30 August, 2017	19:29:11
Cambridge Bay	04 August, 2017	18:37:17	24 July, 2018	18:49:18
Arviat	01 August, 2017	17:31:18	11 July, 2017	17:49:11
Rankin Inlet	03 July, 2017	17:30:42	22 August, 2019	17:49:12
Igloolik	21 August, 2016	17:04:20	17 August, 2019	17:39:11
Iqaluit	20 August, 2017	15:52:06	02 August, 2016	15:59:07

2.3.2 Spectral Data

As no publicly available *in situ* seafloor reflectance information exists from the Canadian Arctic, it was necessary to collect spectral seafloor reflectance data for this project. Cambridge Bay was selected for field data collection due to dive safety consideration and the logistical support available at that site. Field work was completed from August 3 to August 10, 2017, when the region was ice-free. Seafloor reflectance data was collected via SCUBA diving, using an Ocean Optics Jaz spectrometer in a custom waterproof housing unit, with an attached GoPro set to taking photos every 5 seconds, to validate bottom types. A total of two dives were completed, one in each arm of Cambridge Bay. Seafloor reflectance was measured using the panel substitution method, where it is calculated as the ratio of i) the upwelling radiance from the sample target, divided by ii) the upwelling radiance from a Lambertian reference panel (Labsphere, 2011), with correction for non-unity reflectance of the reference panel. We used a calibrated Spectralon reference panel and collected reference measurements approximately every 5 to 10 samples. Three main seafloor types (Figure 2) were identified visually, and a minimum of 100 samples were collected for each type. Collecting seafloor spectra for each study site was not feasible due to limited funding and lack of logistical dive support at the other sites. Consequently, these seafloor types were used for all sites, as they are currently the best available estimate of seafloor spectral reflectance types in the Canadian Arctic.

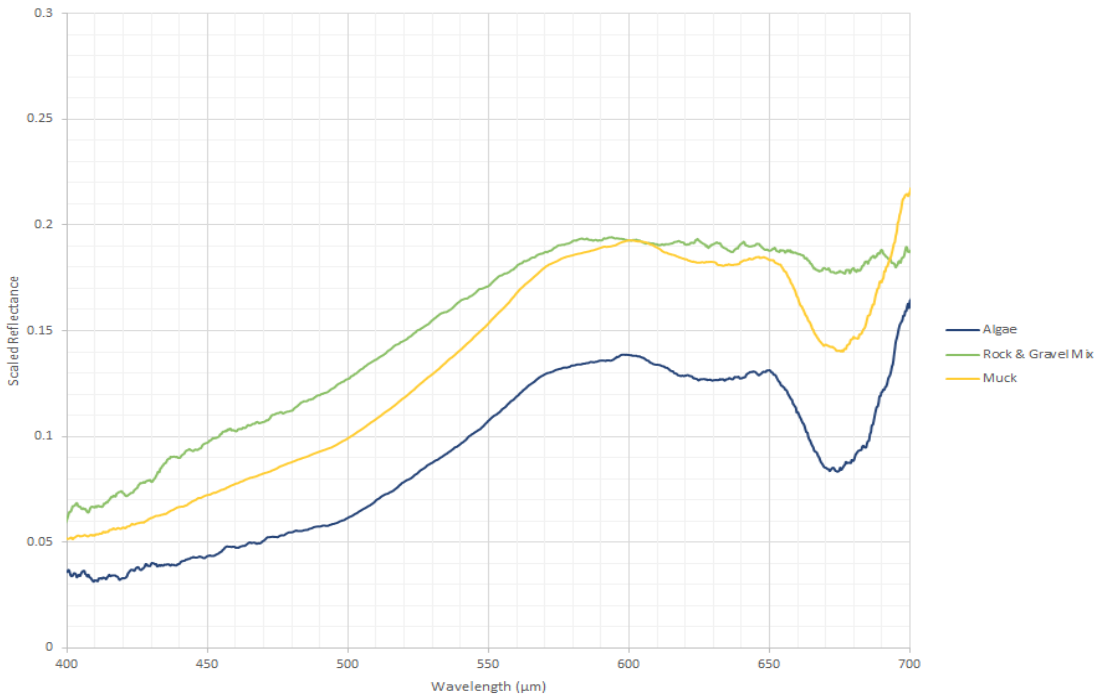

Figure 2 – Three main bottom types determined from dives in Cambridge Bay (Holman & Knudby, 2017).

2.3.3 Depth Data

Bathymetric survey data were acquired for all sites from the Canadian Hydrographic Service (CHS), reduced to Lowest Low Water Large Tide (LLWLT) as per International Hydrographic Organization (IHO) standards (DFO, 2019). These datasets were either collected by acoustic soundings or by airborne lidar bathymetry. Data sets provided by the CHS have an associated Category Zone of Confidence (CATZOC), a metric developed by the IHO to describe data quality using horizontal and vertical accuracy, seafloor coverage, and method used to acquire data to rank quality with "A" being the best (Chenier et al. 2018). These datasets and their relevant information are presented in Table 4 and Table 4 below. Pond Inlet did not have any acoustic data available to us at the time of data collection, rendering calibration of the empirical methods at this study site impossible. As it was found to be unsuitable for SDB given the many complications with environmental factors and acquiring high quality satellite imagery and depth data, Pond Inlet was removed from the study.

Across all remaining sites, the depth data used is the best available temporally and spatially at the time of data collection. Despite this, for most sites, sample points at depths less than 10 m are either missing or limited due to CHS safety guidelines restricting vessels from traveling in water

less than 4 m deep while surveying, known as the Navigable Area Limit Line (NALL) (NOAA 2017). This impacts the results of any analysis attempting to predict depths in these shallow areas. Additionally, only points within the range of 0 – 20 m were used for the project, as deeper water is optically deep for all sites.

Data points that fell outside the image extent were removed. Since Landsat 8 has a larger image extent than the Sentinel-2 L1C product used in this study, some sites had more data points to draw from such as Igloolik or Rankin Inlet. As more data is often better to train the models, this difference between sample points and Sentinel-2 and Landsat 8 was not equalized.

Table 3 – Category Zones of Confidence definitions (IHO, 2018)

ZOC	Position Accuracy	Depth Accuracy	Seafloor Coverage
A1	± 5 m	= 0.50m ± 1% d	All significant seafloor features detected
A2	± 20 m	= 1.00m ± 2% d	All significant seafloor features detected
B	± 50 m	= 1.00m ± 2% d	Uncharted features hazardous to surface navigation are not expected but may exist
C	± 500 m	= 2.00m ± 5% d	Depth anomalies may be expected
D	Worse than ZOC C	Worse than ZOC C	Large depth anomalies may be expected
U	Unassessed	The quality of the bathymetric data has yet to be assessed.	

Table 4 – Collection methods, CATZOC levels, dates of data collection, and the maximum number of data points used per site (Courtesy of CHS, 2016). Points used for calibration and validation may be less depending on image extent.

Community	Collection Method	CATZOC	Year(s) Collected	Dataset Size (Max # Pts)
Kugluktuk	SBES	B	1965-1993	1,712
Cambridge Bay	LiDAR	B	1985	10,239
Arviat	SBES	D	1977	7,198
Rankin Inlet	SBES, MBES	C, A	1975-2010	354
Igloolik	MBES	A	2001-2010	6,603
Iqaluit	MBES	A	2003-2013	6,263

2.4 Methods

Four methods of SDB are compared in this project: three empirical methods and the physics-based approach using two atmospheric correction methods. The individual methods are discussed in sections 2.4.2 and 2.4.3. In general, the steps to estimate bathymetry are as follows:

1. Image pre-processing:
    a. Removal of pixel-to-pixel variations in sun glint
    b. Atmospheric correction
2. Apply water depth estimation algorithm to estimate bathymetry
3. Validate results by comparison to trusted data

The complete workflow for performing SDB using both the empirical and physics-based approaches are presented in Figure 3 below:

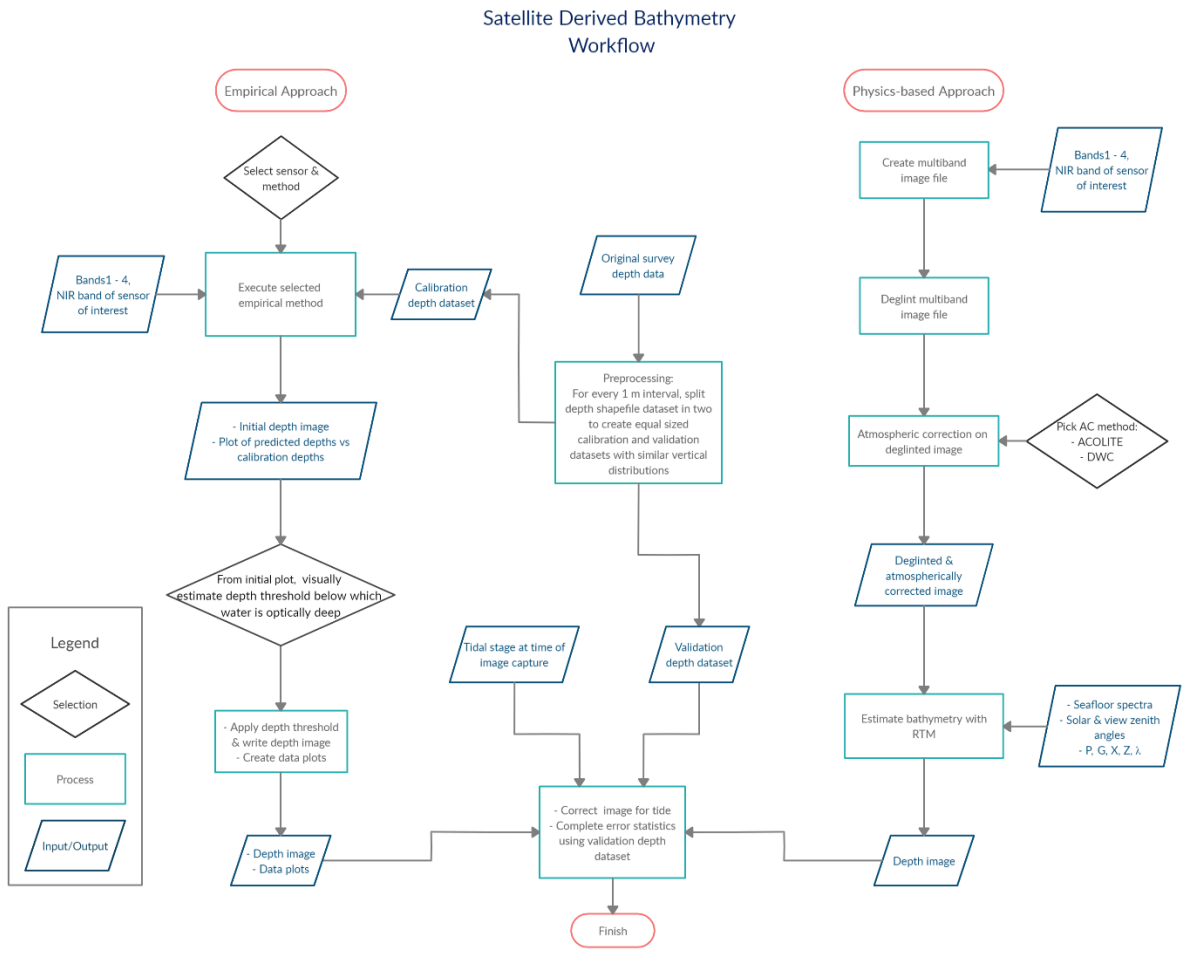

Figure 3 - SDB workflow used for this project.

2.4.1 Image Preprocessing

As the first image processing step common to all SDB methods, units for all images were converted to Top-Of-Atmosphere (TOA) reflectance using coefficients provided in the metadata.

Additionally, for all methods other than the Ratio Transform Algorithm (RTA), all bands in the visible spectrum were used by default for both Landsat-8 and Sentinel-2 (i.e. Bands 1 through 4, or the coastal, blue, green, and red bands respectively), as well as the NIR band (bands 5 and 8 for Landsat and Sentinel respectively) for deglinting imagery for the physics-based method. The coastal band of Sentinel-2 has a 60-m spatial resolution, as opposed to the 10-m resolution of the other visible bands, and is resampled using nearest neighbour to 10 m during processing.

2.4.2 Empirical Approach

All empirical methods rely on deriving a statistical relationship between water depth from the calibration data and pixel colour from the imagery. These methods do not require atmospherically corrected imagery for this relationship to be established, so atmospheric correction was not applied to the imagery used for those methods (Chenier et al., 2018). Additionally, while deglinting the imagery was considered for the project, studies have indicated that in imagery where noise from sun glint reflecting off waves is minimal due to little observed wave action, overall sun glint did not greatly impact SDB accuracy (Chenier et al. 2018). None of the imagery used in this study had visually detectable levels of sun glint, and we therefore did not correct for sun glint as part of the workflow for the empirical methods.

2.4.2.1 Ratio Transform Algorithm

Empirical SDB as pioneered by Lyzenga (1978, 1981) utilized a set of general algorithms based on the use of at least two bands of a sensor to produce information on water depth Z as

$$Z = a_0 + a_i X_i + a_j X_j \quad (1)$$

where

$$X_i = \ln [R_w(\lambda_i) - R_\infty(\lambda_i)] \quad (2)$$

and where R_w is the water-leaving reflectance of a pixel for a band (λ_i) and R_∞ is the water-leaving reflectance of optically deep water for that band. Using acoustic water depth data to tune the algorithm, the coefficients a_0, a_i, and a_j are optimized empirically with a least-squares approach and then used to define the relationship between pixel colour and water depth. This relationship is then extrapolated to all pixels in the image to estimate bathymetry (Lyzenga 1978,

1985). In instances where X_i is undefined (i.e. where $[R_w(\lambda_i) - R_\infty(\lambda_i)] < 0$), depth cannot be estimated. As a result, while Lyzenga's (1978, 1981) method successfully demonstrated the potential to use passive sensors to determine water depth, it cannot map shallow-water areas with lower reflectance than adjacent, optically deep waters, as it implicitly assumes homogeneous water optical properties and seafloor reflectance across the image (Stumpf et al. 2003). It has since been further developed by others to address these shortcomings (Philpot, 1989; Maritorena et al., 1994; Stumpf et al., 2003).

Perhaps the most widely used method to derive water depth using passive optical remote sensing is the RTA, developed by Stumpf et al. (2003). Building on Lyzenga's work, it similarly utilizes georeferenced depth data to establish a statistical relationship between water depth and pixel colour in two bands of a satellite image (typically the blue and green if these are available), and then uses that relationship to estimate per-pixel water depth throughout the image. Stumpf et al. (2003) used a relationship of the form

$$Z = m_1 \frac{\ln(nR_w(\lambda_i))}{\ln(nR_w(\lambda_j)} - m_0 \quad (3)$$

where n is a constant that creates a positive linear response with depth, and m_0 and m_1 are linear transformation parameters (Stumpf et al. 2003). The benefits of using the RTA method are that it can produce reasonable results with even a small dataset, provided that dataset is of high quality (Stumpf et al. 2003). While this method is simple and reasonably effective, it does not consistently produce meaningful results over areas with variable seafloor types or water optical properties, and requires high quality, up-to-date, georeferenced water depth measurements from the area in question (Knudby et al., 2016; Pahlevan et al., 2017; Petit et al., 2017). Despite these shortcomings, the algorithm developed by Stumpf et al. (2003) is still the primary method by which most hydrographic offices perform SDB, and as such is the first of the five methods tested within the scope of this project.

2.4.2.2 Multiband Method

The second empirical method, recently tested in the Arctic by the Canadian Hydrographic Service, is an extension of the original method proposed by Lyzenga (1978, 1985) in equations (1) and (2) (Chénier et al., 2018). The Multiband algorithm uses a multiple linear regression

model with input from several (sometimes all) image bands, each of which are assumed to have a logarithmic relationship with water depth due to exponential attenuation of light in the water column (Chenier et al., 2018). Where the difference between water-leaving radiance R_w and R_∞ is positive, i.e. for optically shallow water, Z can then be derived by:

$$Z = a_0 + \sum_{i=1}^{N} a_1 \ln[R_w(\lambda_i) - R_\infty(\lambda_i)] \quad (4)$$

where the coefficients a_0 and a_i are optimized empirically with a least-squares approach.

2.4.2.3 Random Forest Regression

The third empirical method tested is Random Forest Regression (RFR), a supervised ensemble regression method based on a large number of decision trees. Each decision tree is built from a sub-sample of the calibration data (the collocated pixel values and water depths) drawn with replacement, and the splitting rule used at each node is optimized based on a random subset of the available variables (the image bands). Because of this technique, different data are used to train each tree, which will use different features to make decisions at nodes, which ultimately reduces correlation between the individual decision trees as well as error in the forest (Breiman, 2001). Once the decision trees are generated, for each pixel, each tree provides an estimated depth and the final prediction is produced as an average of the predictions from all trees (Breiman, 2001). Forests were assembled using 100 trees and 50% of the calibration dataset as training data for the machine learning model to build each tree. As with the Multiband method, all bands in the visible spectrum were used by default for both Landsat 8 and Sentinel-2.

2.4.3 Physics-Based Approach

The physics-based approach uses radiative transfer modeling (RTM) to predict remote sensing reflectances for a given combination of water optical parameters, seafloor reflectance, water depth, and environmental factors such as wind speed and view and sun angles. Equation 5 shows this conceptually:

$$R_{rs}(\lambda) \approx f(P, G, X, Z, e(\lambda), \lambda) \quad (5)$$

where the variables are concentration of phytoplankton (P), absorption by gelbstoff at 440nm (G), concentration of suspended particulate matter (X), depth (Z), seafloor reflectance (e), and

wavelength (λ) respectively. This model is then inverted to find the best match to each pixel in the satellite image. The physics-based approach requires, at a minimum, seafloor reflectance spectra (e(λ)) representing the range of seafloor types in the area (Lee et al. 1998), and reasonable ranges of the water quality and depth parameters. This approach also requires satellite imagery to have been corrected for the effects of both the direct sunlight reflected from the sea surface ("sun glint") and atmosphere to produce meaningful results. Within the scope of this project, two different atmospheric correction methods are tested, both using the Advanced Look Up Table (ALUT) approach for forward modeling and the Binary Space Partitioning (BSP) approach for efficient model inversion (Hedley et al. 2009).

2.4.3.1 Deglinting

Deglinting was performed using the method developed by Hedley et al. (2005), based on the Top-Of-Atmosphere (TOA) reflectance (R_{TOA}) values in each band. With this method, homogenous deep-water sample areas displaying a range of sun glint are selected, the minimum NIR R_{TOA} of these areas is established ($\mathrm{Min}_{\mathrm{NIR}}$), and a linear regression of NIR R_{TOA} against the $R_{TOA}$of each of the visible bands performed. With b_i as the slope of the regression line for visible band i, the glint-free brightness of each pixel, R'_i is then found as:

$$R'_i = R_i - b_i(R_{\mathrm{NIR}} - \mathrm{Min}_{\mathrm{NIR}}) \quad (6)$$

where R_i is the pixel R_{TOA} in band i, R_{NIR} is the pixel R_{TOA} in the NIR band.

2.4.3.2 Atmospheric correction

Two atmospheric correction models were tested in this project: ACOLITE (Vanhellemont & Ruddick, 2016), and the Deep Water Correction (Hedley, 2018). ACOLITE is an atmospheric correction algorithm and software developed for coastal and inland water applications by Vanhellemont (2019) and Vanhellemont & Ruddick (2014, 2015, 2016, 2018) for Landsat 5/7/8 and Sentinel-2. ACOLITE assumes that the water-leaving reflectance is zero in the SWIR bands, which means that the aerosol reflectance can be assumed equal to the Rayleigh-corrected reflectance in the SWIR wavelengths (Vanhellemont & Ruddick, 2016). In other words, the signal in the SWIR bands that remains after Rayleigh correction is assumed to come exclusively from aerosol scattering (Vanhellemont & Ruddick, 2016). The ratio of the aerosol reflectance in

the two SWIR bands can then be extrapolated with an atmospheric model to the visible and NIR bands (Vanhellemont & Ruddick, 2016).

The second method is based on recent work by Hedley (2018), who developed a new approach for atmospheric correction specifically for SDB applications. Using fixed atmospheric and aerosol models, this method uses user-outlined deep-water areas to optimize two parameters: the aerosol optical thickness (τ_{550}) and the near-surface wind speed (u_{10}). Using a combined atmospheric correction and bathymetry estimation process, these two parameters are optimized to produce deep bathymetry estimates for the deep-water areas (Hedley, 2018). First, a LUT with deep-water remote sensing reflectance (R_{rs}) values is built using the same water quality parameters as in (5) and depths > 30 m. Using iteratively optimised τ_{550} and u_{10} values, the squared difference between image-derived R_{rs} values produced by the AC and the modeled R_{rs} values in the LUT is then minimized to find the optimal values of τ_{550} and u_{10} (Casal et al., 2020). These values are then used to perform the AC for the entire image (including < 30 m water) (Casal et al., 2020).

2.4.3.3 Bathymetry estimation

Semi-analytical equations (Lee et al. 1998, 1999) developed from thousands of runs of the HydroLight radiative transfer modeling (RTM) software were used to produce Look Up Tables (LUTs) containing the parameters mentioned above (P, G, X, Z, $e(\lambda)$, and λ) as well as the R_{rs} each parameter combination would produce (Mobley et al., 2005; Petit et al., 2017). The LUT is then compared to each image pixel, and the depth corresponding to the best match is allocated to each pixel. A critical issue for this approach is the large amount of time it requires to invert large LUTs, combined with the fact that differences in R_{rs} due to differences in water depth and seafloor reflectance become exponentially smaller with increasing water depth (e.g. given constant water quality, a bright seafloor looks nearly identical under 25 m or 1000 m of water, but quite different under 10 m of water). To speed up the LUT creation and the model inversion process, adaptive look-up tables (ALUTs) were used. Construction of an ALUT is accomplished by first running initial models using different parameter value combinations to fully cover the parameter space of a voxel of *n* dimensions (Knudby et al., 2016). Within the parameter space, the most undersampled region, or the region with the greatest mean Euclidean distance between spectra on opposing sides of the voxel, is searched and split into equal parts creating two new

voxels. This process is then repeated a pre-defined number of times to cover the full spectral space with the desired level of discretization (Knudby et al., 2016). This has the effect of reducing discretization error for a LUT of a given size (Hedley et al., 2009). Once the ALUT is built, a Binary Space Partitioning (Hedley et al. 2009) approach is used to search through it efficiently and identify the R_{rs} spectrum that most closely matches that of each pixel. The water depth (Z) used in the forward model to produce that spectrum is then assigned as the water depth estimate for the pixel.

2.4.4 Validation

All lidar and acoustic data for each site were stratified into 1-metre depth intervals, and data in each depth interval were then split randomly into two equally-sized subsets. Separate calibration and validation data sets were then created by combining one of the two subsets from each depth interval. The calibration data were then used to train the empirical methods, and the validation data were used for testing the performance of all methods. Predicted depths for each method were compared against the validation datasets, and the Mean Absolute Error (MAE)[1] and bias were calculated based on those results in 2 m intervals up to 20 m, and for the entire range of 0 – 20 m as well.

2.5 Results

Cambridge Bay and Kugluktuk had sample points that were well distributed both horizontally and vertically, allowing SDB performance to be assessed at both sites. These two sites produced dramatically different results due to environmental characteristics and data quality, as presented in detail below. Results for Sentinel-2 and Landsat-8 images were very similar, with Landsat-8 performing slightly worse; only results based on the Sentinel-2 data are presented here. All results produced for both sensors at all sites can be found in Appendix A. Scatter plots produced compare observed and predicted depths, and are assessed based on a 1:1 relationship between the two datasets.

[1] The data that the reported SDB results are compared to, derived with acoustic or lidar instruments, are arguably estimates themselves. The validation exercise may thus be understood better as a quantifying a difference, rather than the of the error SDB results. For this report, the term ‘error’ is used in the common way to mean a difference between a water depth derived from SDB and another water depth derived from the validation dataset.

2.5.1 Cambridge Bay

Out of all the sites, SDB for Cambridge Bay produced the lowest overall mean absolute errors. Over a range from 0 to 20 metres, of the different methods tested, RFR produced the lowest MAE of 1.12 m. In waters less than 2 m deep, MAE values ranged as low as 0.38 m using RFR, up to 0.77 m using ACOLITE method for the physics-based approach. The DWC physics-based method also produced low MAE of 0.44 m in the 0 – 2 m range, but errors increased quickly with depth to produce the largest overall MAE of 2.62 m. The RFR method has a lower MAE than all other methods in water < 10 m deep. In general, most results had MAE values of < 2 m in each interval, except DWC for which MAE increased up to 4.04 m between 4 – 14 m depths, after which it decreased again. Table 5 provides all MAE values achieved across the 0-20 m depth range for all methods, at Cambridge Bay.

Bias derived from RTA and RFR was very close to 0, ranging between - 0.43 and +0.51 m for the RTA method and between -0.13 and +0.26 m for RFR. The Multiband method also produced relatively low bias, though slightly higher than either of the other empirical methods, and with exceptions in the 12 – 14 and 18 – 20 m ranges (-1.33 m and +1.74 m respectively). Both physics-based methods produced much higher bias, ranging from -1.57 to +2.88 m, though ACOLITE tended toward a negative bias as opposed to the large positive bias observed in DWC.

Table 5 – Cambridge Bay bias and Mean Absolute Error results.

Depth Intervals	Ratio Transform Algorithm		Multiband Method		Random Forest Regression		ACOLITE		Deep Water Correction	
(m)	Bias	MAE	Bias	MAE	Bias	MAE	Bias	MAE	Bias	MAE
0 – 20	0.00	1.27	-0.05	1.33	-0.01	1.12	-0.37	1.74	1.90	2.62
0 – 2	-0.43	0.54	-0.60	0.72	-0.11	0.38	-0.75	0.77	-0.37	0.44
2 – 4	-0.01	0.85	0.39	0.93	-0.10	0.69	-1.03	1.31	0.50	0.86
4 – 6	0.06	1.14	0.52	1.23	-0.03	0.79	-1.57	1.70	1.06	1.31
6 – 8	0.10	1.18	0.15	1.24	-0.03	0.98	-0.96	1.52	1.91	2.16
8 – 10	0.37	1.14	-0.31	1.31	0.02	0.99	-0.62	1.45	2.61	3.07
10 – 12	0.48	1.51	-0.70	1.75	0.20	1.39	-0.85	2.03	2.88	3.56
12 – 14	-0.16	1.59	-1.33	2.03	-0.13	1.65	-0.24	2.01	2.55	4.04
14 – 16	-0.39	1.74	-0.46	1.81	-0.06	1.61	-0.52	2.04	2.48	3.45
16 – 18	-0.41	1.55	0.04	1.66	0.02	1.61	0.50	2.10	1.74	2.52
18 – 20	0.51	1.23	1.49	1.74	0.26	1.13	2.28	2.39	1.75	2.06

Scatter plots of SDB-derived against validation depths indicate a generally linear relationship for all three empirical methods, and for the ACOLITE RTM method within 0 – 10 meter depths, and, as expected, an increase in error with depth for all methods (Figure 4). The DWC method performs well in very shallow and very deep waters, but substantially overestimates depths in the 5 – 15 m depth range. Banding appears in the ACOLITE scatter plots (at all sites) as an artefact of the ALUT process, which does not resolve small depth differences in deep water.

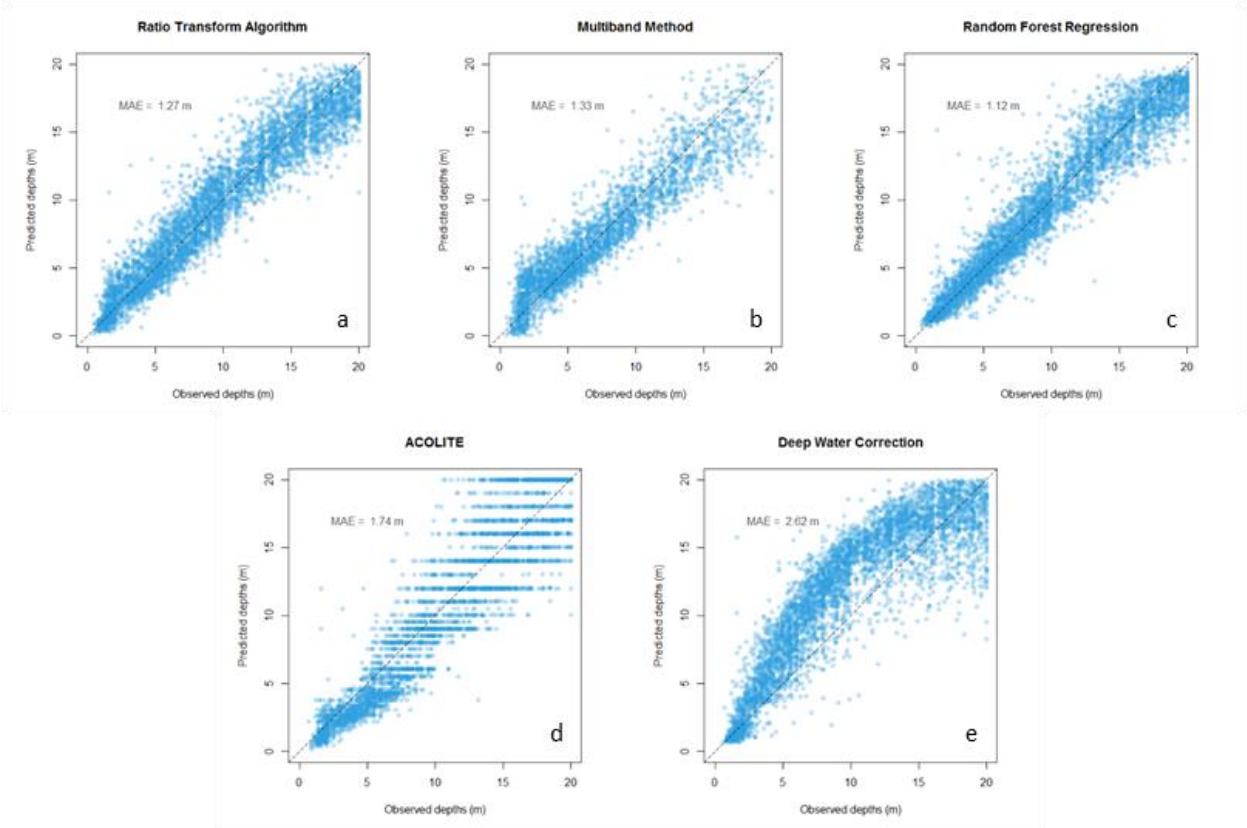

Figure 4 – Ratio transform algorithm (a), multiband algorithm (b), Random Forest regression (c), RTM using ACOLITE (d) and the Deep Water Correction method (e) results up to 20 metres in Cambridge Bay. MAE is calculated for the entire 0 – 20 m range.

Bathymetry images produced from each method are provided in Figure 5 below. Based on visual assessment, all the methods are able to identify bathymetric features at Cambridge Bay relatively well, with the exception of the Multiband image (5e), which makes no predictions when $R_w(\lambda_i) - R_\infty(\lambda_i)$ from Equation 4 results in a negative number, i.e. when the pixel is darker than what has been defined as optically deep within the image by the plugin. Those pixels are returned as "NoData" values.

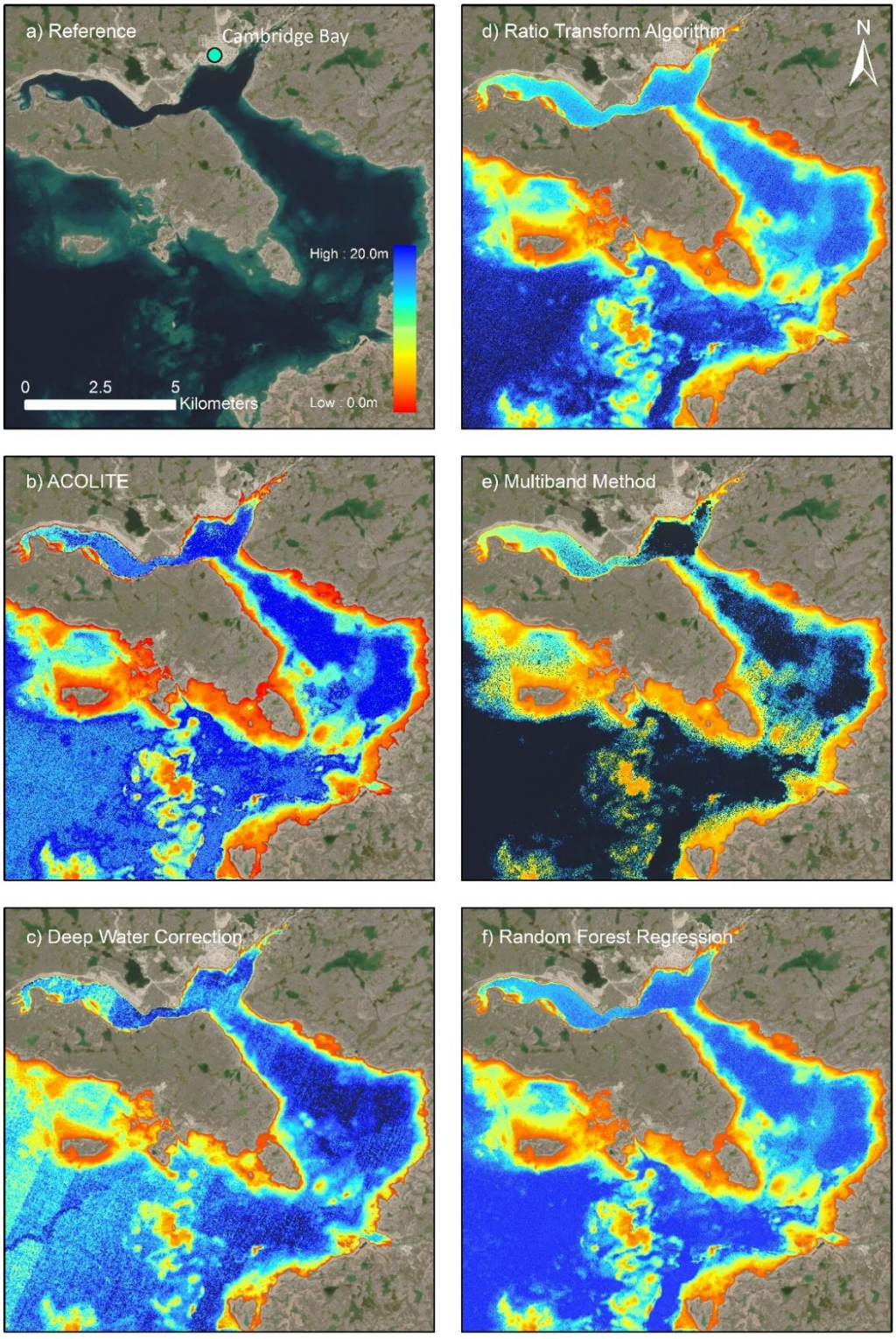

Figure 5 – Bathymetry products from SDB analysis at Cambridge Bay.

2.5.2 Kugluktuk

Kugluktuk results varied widely across method and depth and are presented in Table 6. Generally, the best results were achieved in water less than 4 m deep and using the empirical methods. Beyond 4 metres, results vary dramatically between methods and error increases quickly with depth. Despite this general pattern, RFR still produces the lowest overall MAE values in the 0 – 20 m range (1.89 m) of all methods tested and typically had among the lowest values, if not the lowest, in each depth interval. In the 0 – 2 m range the lowest MAE was 0.57 m using the ACOLITE RTM method, though it was 3.56 m overall in the 0 – 20 m range. It should be noted that 54% of the validation points were in the 0 – 4 m range, influencing overall MAE results in the 0 – 20 m range. Errors for each 2 m interval beyond 4 m were generally higher, often greater than 2 m and as high as 13 m. No regular error distribution is observed in these results. The 18 – 20 m range using DWC returned no values measured due to an absence of depth values predicted in that range.

Bias values measured at Kugluktuk are typically close to zero in depths less than 2 m, then become irregular for all methods in both positive and negative directions. The greatest variance is produced by the physics-based methods, especially DWC, with bias ranging from -0.12 m to

Table 6 – Kugluktuk Bias and Mean Absolute Error results.

Depth Intervals	Ratio Transform Algorithm		Multiband Method		Random Forest Regression		ACOLITE		Deep Water Correction	
(m)	Bias	MAE	Bias	MAE	Bias	MAE	Bias	MAE	Bias	MAE
0 – 20	0.08	2.50	0.17	1.43	-0.41	1.89	0.90	3.56	-0.97	3.97
0 – 2	-0.51	0.90	-0.17	0.64	-0.30	0.63	0.56	0.57	-0.12	1.19
2 – 4	1.23	1.67	1.03	1.40	0.51	1.12	1.27	1.40	-4.45	5.18
4 – 6	1.91	2.66	0.87	2.09	0.07	1.90	2.52	3.01	-4.71	6.35
6 – 8	1.11	2.67	0.36	1.50	-0.64	2.97	4.99	5.25	-2.96	5.75
8 – 10	-1.59	3.39	-1.94	2.74	-2.02	3.39	0.16	3.79	-0.15	4.75
10 – 12	-1.24	4.19	-0.54	2.42	-1.61	3.92	-1.65	4.05	2.63	6.05
12 – 14	-0.71	3.27	-1.73	3.19	-0.80	3.39	-3.28	3.38	3.21	5.40
14 – 16	-1.05	3.01	-0.38	1.32	0.39	2.88	6.46	8.41	1.80	4.23
16 – 18	1.40	3.15	1.64	3.77	0.42	2.85	0.69	3.11	13.0	13.0
18 – 20	1.84	2.23	0.64	1.59	2.73	2.73	4.72	4.72	NA	NA

+13 m, albeit the latter was derived from very deep water. ACOLITE tended to overestimate depths at Kugluktuk, whereas DWC first underestimates depths up to 10 m, then overestimates thereafter.

The scatter plots of SDB-derived depths against validation depths also reflect this (Figure 6). Each indicate clustering of validation points in the 0 – 3 m range, but little correlation is observed beyond that, though it is noted that the empirical methods appear to perform better at depths > 3 m.

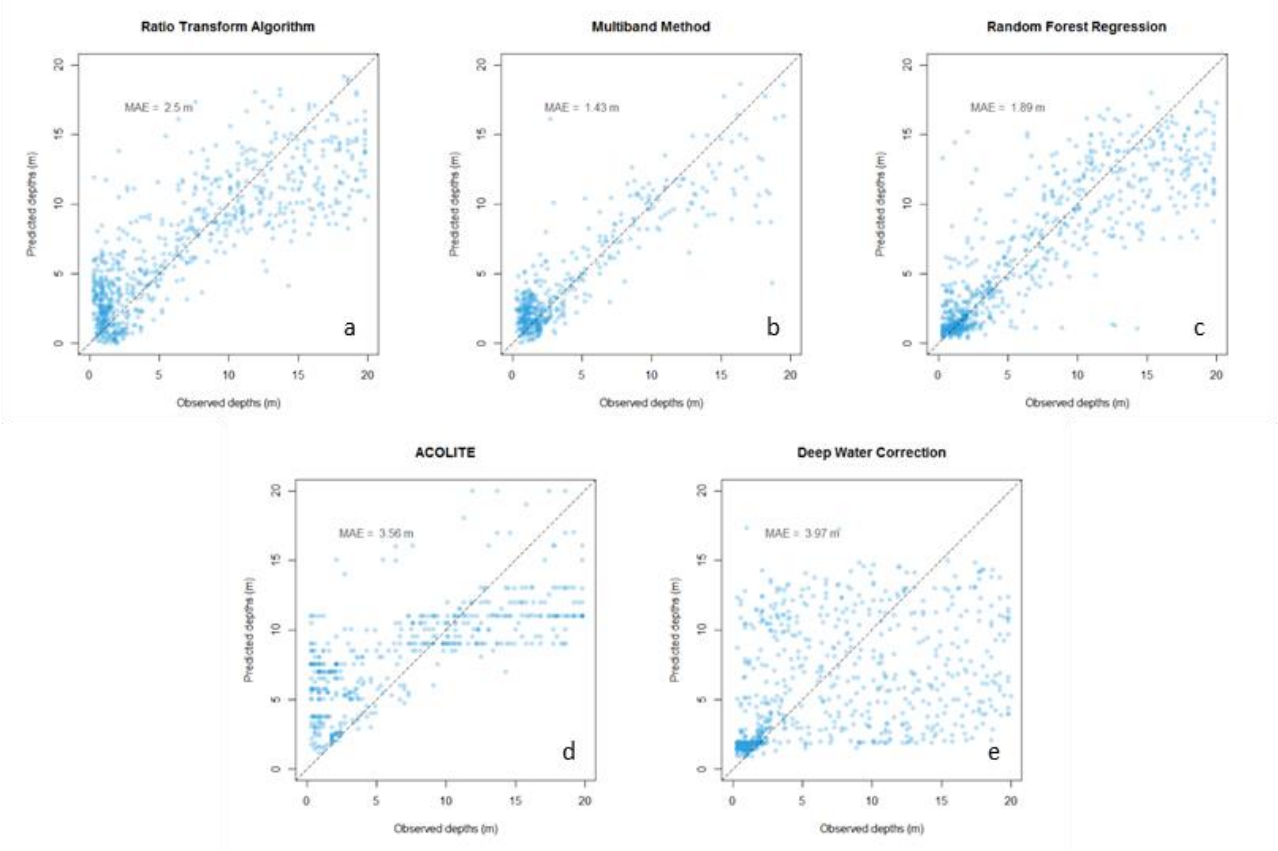

Figure 6 - Ratio Transform algorithm (a), Multiband method (b), Random Forest regression (c), RTM using ACOLITE (d) and Deep Water Correction (e) results up to 20 metres in Kugluktuk. MAE is calculated for the entire 0 - 20 m range.

Bathymetry images produced from each method are provided in Figure 7 below. The nearshore area around Kugluktuk is clearly identified by all methods except Multiband (7e), which again returns "NoData" when $R_w(\lambda_i) < R_\infty(\lambda_i)$ (Equation 4). Bathymetry features are seen in the top left corner of all the images though with great variation, where suspended sediments may be

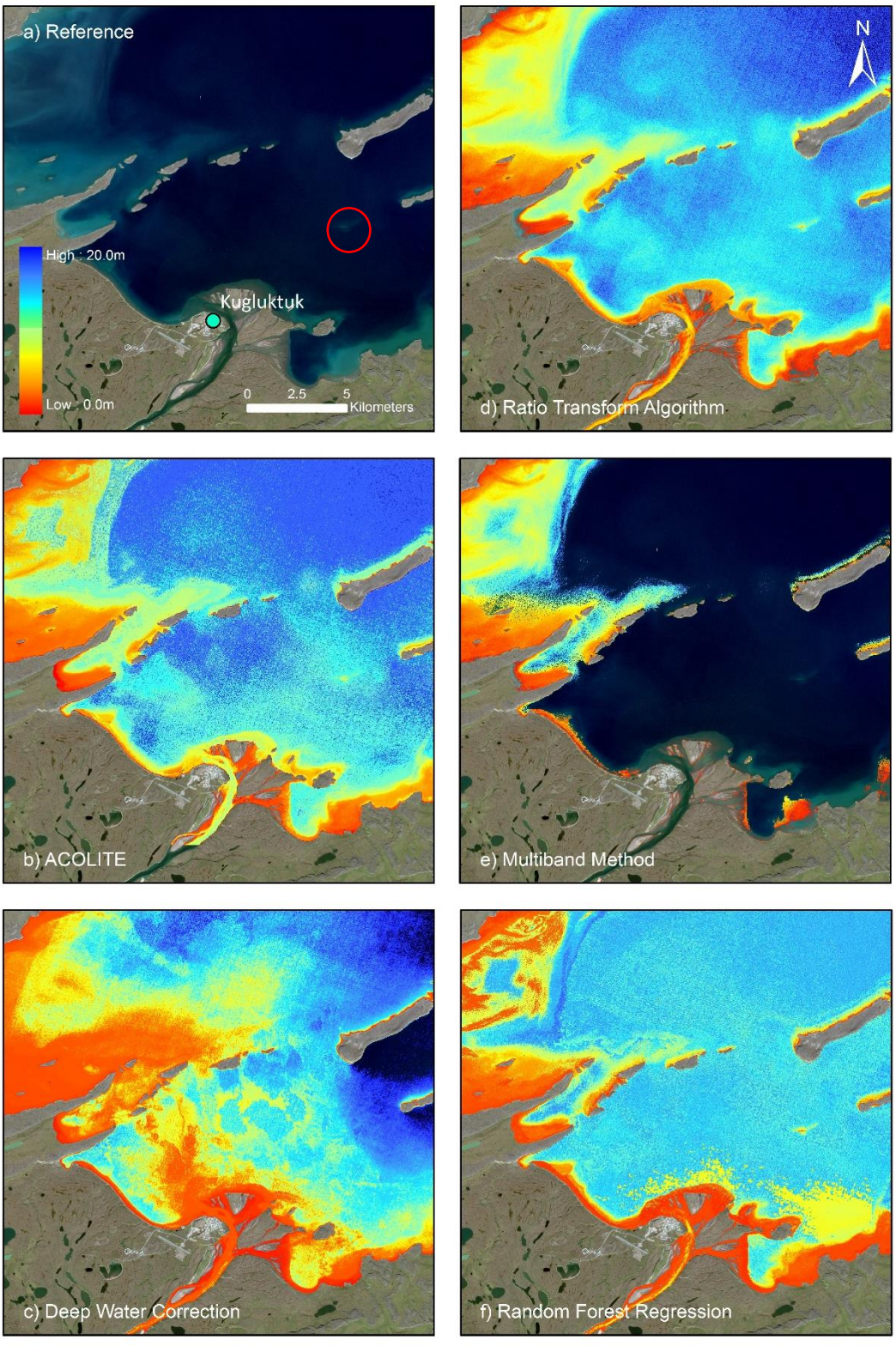

Figure 7 - Bathymetry products from SDB analysis at Kugluktuk. The red circle in 7a indicates the location of a shallow feature identified in 7b, 7d, and 7f that is otherwise difficult to observe.

mistaken for shoals. Figure 7a also indicates where a shallow feature is not easily observed from the true colour image, but is identified in the SDB products by the ACOLITE (7b), Ratio Transform (7d), and Random Forest (7f) methods. In most cases, and with the exception of the immediate nearshore areas, common bathymetry features are tenuously identified at best, particularly in areas with higher variability in bathymetry or turbidity.

2.5.3 Arviat, Rankin Inlet, Igloolik & Iqaluit

Results for the remaining sites varied widely between methods. MAE at Arviat ranged from 0.91 m using DWC to 10.7 m using ACOLITE, and bias ranged from -10.7 m using ACOLITE to +3.92 m using Multiband. MAE at Rankin Inlet ranged from 1.78 m using Random Forest to 15.3 m using ACOLITE, and bias ranged from -15.3 m using ACOLITE to +2.40 m using Ratio Transform. No predictions were made at depths shallower than 14 m by the empirical methods at this location or Igloolik. Igloolik MAE ranged from 0.08 m using Random Forest to 2.81 m using DWC, and bias ranged from -15.3 m using ACOLITE to +4.10 m using DWC. Despite no predictions being made in shallow water at this location, bias remained near zero and MAE ranged from +0.02 m to +1.35 m within the empirical methods. Lastly, Iqaluit MAE ranged from 0.68 m to using Random Forest to 5.56 m using DWC, and bias ranged from -5.37 m using DWC to +4.67 m using Multiband.

In general, Random Forest MAE tended to be lower at all sites, whereas ACOLITE and DWC typically had the highest MAE. Lower bias was observed using the empirical methods, particularly Ratio Transform and Random Forest. Possible reasons for the erratic results observed at these sites are discussed further below.

2.6 Discussion

A number of factors influence data quality, both for satellite imagery and water depth data, which in turn may influence the results of SDB in general. These include:

1) Image and environmental factors
    i. Solar zenith angle
    ii. Water quality
    iii. Presence/absence of clouds, ice, wind, and sun glint

2) Quality of geolocated water depth data
    i. CATZOC level, which relates to the geolocation accuracy of the data points
    ii. Distribution of data points, both vertically and horizontally

Specifically, low solar zenith angles and an absence of clouds, ice, wind, and sun glint all serve to improve visibility and brightness of the seafloor, which is crucial for accurate SDB. CATZOC level ‘A’ or ‘B’ datasets ensure that the water depth data have good positional accuracy, and good data distribution across the depths of optically shallow water ensure good calibration of the empirical models, and good validation of both empirical and physics-based models.

Due to the scope of this project, a considerable volume of results was produced, but poor calibration/validation data at several sites made the quality of many of the results difficult to assess. Additionally, the quality of the satellite images used may have contributed to the quality of results as well. For example, Kugluktuk and Arviat appear more turbid in areas of the imagery, whereas Cambridge Bay and Igloolik appear completely clear by comparison. Despite this, the images produced may still be used for qualitative assessments. Calibration data and the performance of each approach are evaluated further.

2.6.1 Calibration Data

For the empirical methods, the quality, quantity, and depth distribution of the calibration data were critical to producing reasonable results. As a consequence, the only conclusion that can be drawn from applying the empirical methods to several of the sites (i.e. Kugluktuk, Arviat, Rankin Inlet, Igloolik, and Iqaluit) is that the calibration data were insufficient to produce a reasonable result for these sites, either because the data were out of date, data collection methods were unreliable, the data lacked shallow-water sample points, the horizontal or vertical distribution of sample points was insufficient, or some combination of the above. For example, much of the data for Kugluktuk was collected in 1965 using a single-beam echo sounder. At the time, SBES technology was still relatively new and required manual operation by an attentive user to conduct the survey. The hamlet of Kugluktuk itself is situated on a river delta that appears to have a high sediment load, which could change the morphology of the region in the ~50-year period between the survey and the satellite image acquisition. Similarly, Arviat and Rankin Inlet (partially) both use older SBES data from 1977 (just prior to the invention of GPS). Igloolik and

Rankin Inlet completely lack calibration data at depths less than 10 m, while Iqaluit has very few. All three have what is considered high quality datasets (CATZOC level 'A') but the lack of shallow water calibration points resulted in no predictions in these depths, and while bathymetry was mapped for these sites and results were validated quantitatively, it was not meaningful to do so.

Cambridge Bay and Kugluktuk had many shallow-water data points, but Kugluktuk had only 1,685 points[2] covering an approximate area of 35 km², while the data used for Cambridge Bay is well distributed across the site as well as through the water column, with a total of 10,239 points covering an approximate area of 114 km². A breakdown of points within each depth range at Cambridge Bay and Kugluktuk is shown in Table 7 below. While Cambridge Bay has fewer sample points in the 0 – 2 m range than its other depth ranges, there are still many sample points in water less than 10 m deep. More data points allow for better training the algorithms to estimate bathymetry, as well as for validation of their accuracy, though a small number of data points does not necessarily preclude the algorithms from making good estimates.

Kugluktuk datasets were collected using SBES in 1965 and 1993 and are CATZOC level B, which has a horizontal accuracy of 50 m and a worst allowable vertical accuracy of ± 1.2 m

Table 7 – Calibration data sample point distributions across depths.

	Number of Calibration Points	
Depth Range (m)	Cambridge Bay	Kugluktuk
0 – 2	373	330
2 – 5	897	147
5 – 10	1606	123
10 – 20	2178	235

between 0 – 10 m, and ± 1.6 m between 10 – 30 m (IHO, 2018). The Cambridge Bay dataset was collected in 1985 and is also CATZOC level 'B'. At the time of data collection in Kugluktuk, positional errors for data collected with an SBES in 1965 were likely relatively high, given the lack of GPS at the time, and echo sounding technology itself was still in its infancy. While both

[2] Total points ≤ 20 m, prior to splitting into calibration and validation datasets.

datasets are of the same class according to IHO standards, the lidar data from Cambridge Bay appears to be much higher quality as good results were produced across all methods using the Sentinel-2 image.

Kugluktuk also has a relatively higher amount of suspended sediment in its adjacent waters. Turbidity is highest nearshore but is also mixed unevenly throughout deeper waters, rendering SDB methods more prone to error as the empirical methods assume homogeneous water quality throughout the area, and all methods rely on a non-negligible part of the water-leaving radiance to have originated as reflectance off the seafloor. Methods that were successful in estimating depth in Kugluktuk were only successful in water less than 4 m deep, as is seen in the DWC and RFR plots from Figure 6e and 6c respectively, but even these depths had MAEs up to 1.19 m in the 2 – 4 m range. Visual investigation of the satellite imagery indicates a steep drop-off nearshore, where uneven sediment distributions caused by water mixing lead to turbid waters being misinterpreted as shallow water. Examples of this are found in Figure 7, where all methods, to varying extent, identify what is clearly a plume of suspended matter from the river as shallow water. Figure 8 shows the data distribution and imagery used to make predictions, as well as the sediment load in Kugluktuk.

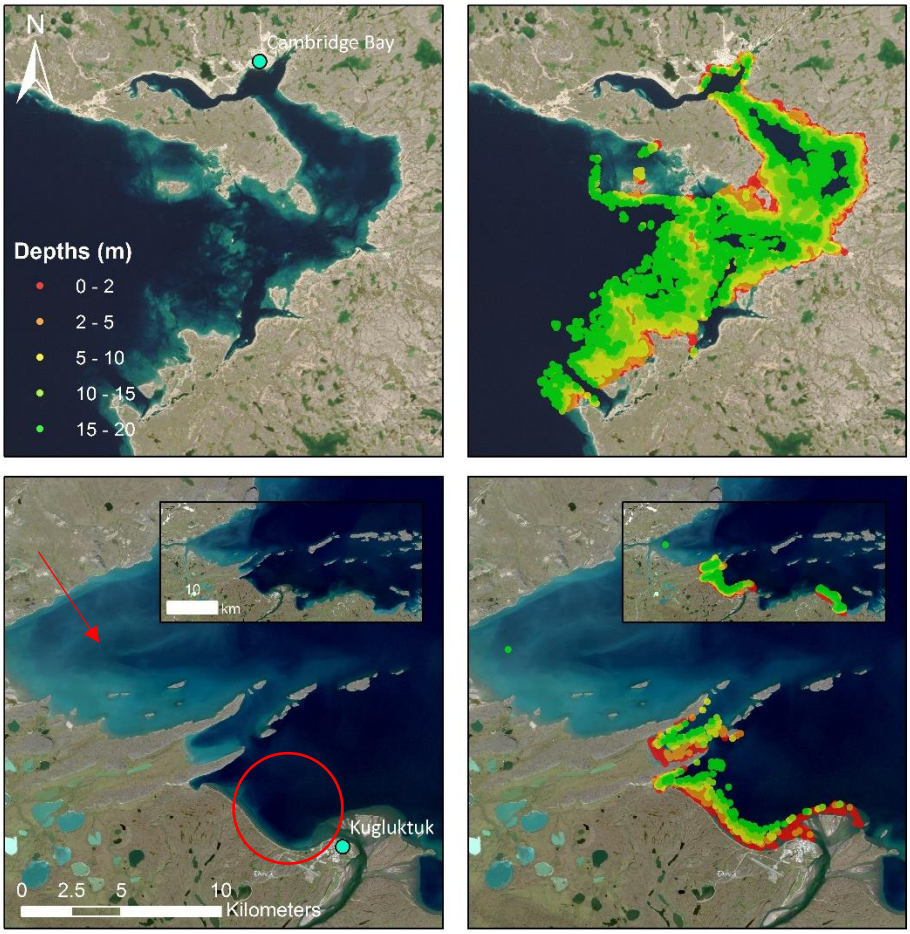

Figure 8 - Comparison of area coverage between Cambridge Bay (top) and Kugluktuk (bottom). Image scale is the same for both locations. Cambridge Bay had several thousand more data points that were evenly distributed across the area, covering many changes in seafloor type and depth. Data for Kugluktuk is limited to two small regions with some additional points scattered through the region, and is impacted by sediment produced from the river that Kugluktuk is situated on, circled in the figure, as well as variable bottom types which produced mixed results, indicated with the arrow.

2.6.2 Empirical Methods

Across all the sites, RFR outperformed the more commonly used empirical methods. One reason this may be the case is that both the RTA and Multiband methods make predictions based on a logarithmic relationship that assumes exponential decay of light through the water column as well as homogeneous water quality and seafloor reflectance. While the assumption of exponential decay is reasonable in the middle water column of deep-water areas, it breaks down near the seafloor due to multiple scattering from the bottom, and near the water surface due to refraction from waves (Newman & LeDrew, 2001). The RTA method also performs poorly in areas with high variability in water quality, seafloor reflectance, or atmospheric conditions, as it implicitly assumes these factors are homogeneous throughout the site, which is rarely the case

(Casal et al., 2020). Newman & LeDrew (2001) determined that an SDB algorithm that is able to account for changes in the attenuation of light with depth, as well as changes in bottom types, would increase confidence in results from SDB analysis, though such an algorithm has yet to be derived.

RFR performs better that the RTA and Multiband methods, possibly due to the ensembling technique that it employs, which ultimately leads to better results in all intervals. Even in Igloolik where there were no shallow-water calibration data, the dataset itself was reasonably large and of high quality (CATZOC level 'A'). A modest linear relationship is identified using the Sentinel-2 image, and a strong relationship is identified using the Landsat-8 image, despite increased noise in deeper water (Figure 9a and 9b). By contrast, Rankin Inlet had the fewest number of sample points to train the RFR model. Despite this, the Landsat 8 image results also produced a modest linear relationship (Figure 9c). Performance was poorer using the Sentinel-2 image (Figure 9d), though this can be attributed to poor image quality or fewer calibration data points to train the models due to the smaller image extent of the Sentinel-2 image.

The Multiband method was expected to produce results of similar quality to the RTA method but tended to underperform at all study sites when comparing bathymetry products as well as error (Figures 4 – 7). This is potentially due to the method by which $R_\infty(\lambda_i)$ from Equation 4 is found, or the combination of bands used to perform the analysis. Previous studies have tested to find the optimal band combinations on a per-site basis (Chénier et al., 2018), though this was intentionally not done for this project as all of the visible bands are assumed to contribute information at different depths, and therefore valuable for general purpose use within the framework of the QGIS plugin.

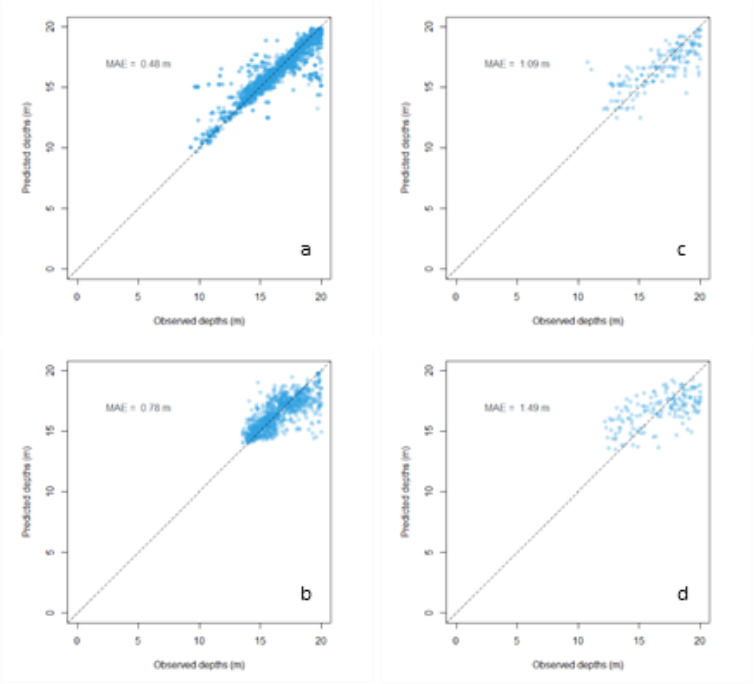

Figure 9 – Random Forest Regression results at Igloolik (a & b) and Rankin Inlet (c & d) for both Landsat 8 (top) and Sentinel-2 (bottom). Despite the complete absence of shallow water depths, it was still able to make reasonable predictions in deeper waters, though noise is greater in such depths.

2.6.3 Physics-Based Methods

Accurate atmospheric correction is critical for the physics-based approach to SDB. Despite the lack of dedicated atmospheric correction models for the Arctic, in general results varied dramatically between methods, sites, and depth intervals. Moreover, sites where validation data are few or of poor quality are difficult to draw conclusions from, as the two methods may in fact have produced results that are better (or worse) than the validation data. This underscores the need for high quality depth data for validation of SDB.

Despite these challenges, ACOLITE tended to produce lower MAE where it was able to form a tentative linear relationship, though overall error tended to be much greater in areas where it clearly failed such as at Igloolik using the Sentinel-2 image (see Appendix A for complete results). Both methods appear to be biased in opposing directions. DWC nearly always overestimates intermediate depths as shown in Figure 10 at Cambridge Bay, skewing overall MAE, but errors in very shallow or very deep depth intervals tend to be lower than the corresponding intervals of ACOLITE. Research is ongoing to identify the cause of this problem and correct the resulting overestimation of intermediate-depth water.

Both ACOLITE and DWC produce images that identify shallow bathymetry features well (Figure 11). DWC appears to be more sensitive to suspended matter, as is shown in Figure 11 at Kugluktuk, where it appears to have mis-identified a plume of suspended sediment as shallow water. This is also the case for the RTA and Multiband methods, to a lesser extent. In areas with poor quality validation data, bathymetry features are still well identified, such as in Arviat, Iqaluit, and Igloolik (Figure 12). In each of these images, the depths

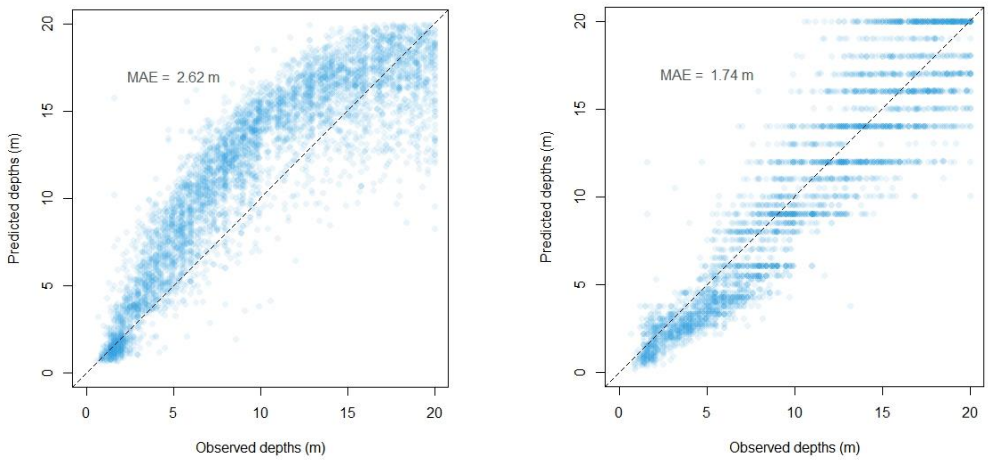

Figure 10 – DWC (left) and ACOLITE (right) results for Cambridge Bay. A linear relationship is established in very shallow waters, curves away, then returns to the 1:1 line, skewing overall MAE with the DWC method. ACOLITE appears to perform much better as a result, though MAE results in the 0 – 2 m and 2 – 4 m depth intervals are better using DWC. This trend is seen for most sites where ACOLITE performs better than DWC.

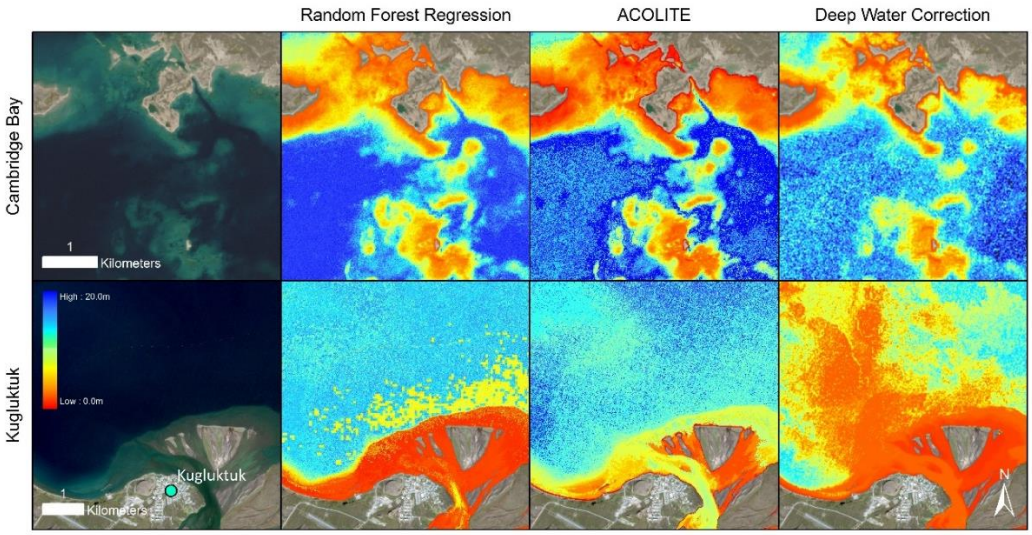

Figure 11 – Results comparison of areas with higher depth variability in Cambridge Bay (top) and Kugluktuk (bottom).

are unverified but clearly indicate areas where shallow features are located, even with suspended sediment confusing some of the areas as in Arviat (circled).

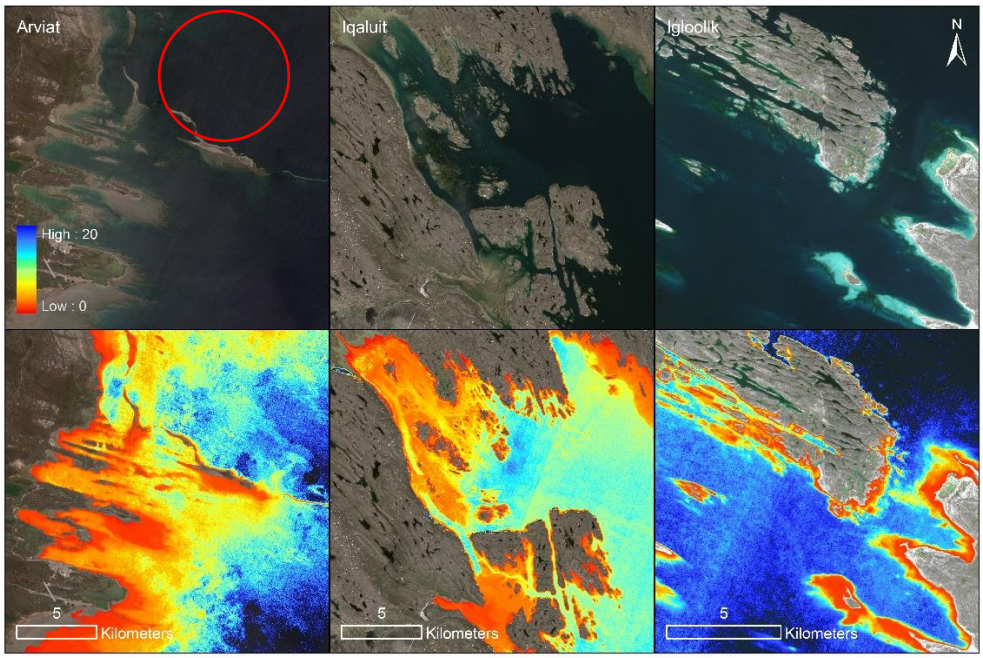

Figure 12 – Shallow bathymetry features identified by the DWC method in areas with poor quality validation data.

2.6.4 Empirical vs Physics-Based Methods

Data used for calibrating the algorithms and subsequently validating the results were largely insufficient in quality, making interpretation of results and comparing methods challenging. Better predictions are expected to be possible with the availability of new acoustic data from CHS. Nonetheless, of all the methods tested here, RFR appears to be the most consistent method and regularly produces good results - when sufficient and suitable calibration data are available. However, most of the Arctic still lacks sufficient calibration data to train empirical SDB models, leaving the physics-based approach as the only option. For Cambridge Bay, the site with the best data available to assess the methods, the physics-based methods generally had larger errors, and the DWC method substantially overestimated intermediate depths. This is likely because the precise atmospheric correction needed for the physics-based approach remains a challenge, especially in the Arctic where ice-free imagery is only available when the sun is relatively low on the horizon. While quantitative assessment of SDB performance is not meaningful in areas with poor validation data, visual assessment suggests that physics-based SDB, despite its larger errors, still produces valuable insights into landscape-scale bathymetry and feature identification.

The Rankin Inlet site provides a great example of this – it has the fewest calibration/validation points of all the sites and the few data available are of poor quality. The empirical methods perform very poorly as a result, but many bathymetric features are clearly identified in the DWC images where no survey data exists, as is shown in Figure 13 where DWC is compared against RFR. These shallow rocky features are difficult to identify in the true colour image and are not covered by the acoustic survey at the site, but constitute a real danger to shipping in the area. An exact depth is not yet possible to verify according to IHO charting standards; nonetheless, the visual interpretation of such an image produced for an area with no chart data is a worthwhile tool for navigation to reduce risk to marine vessels and the environment.

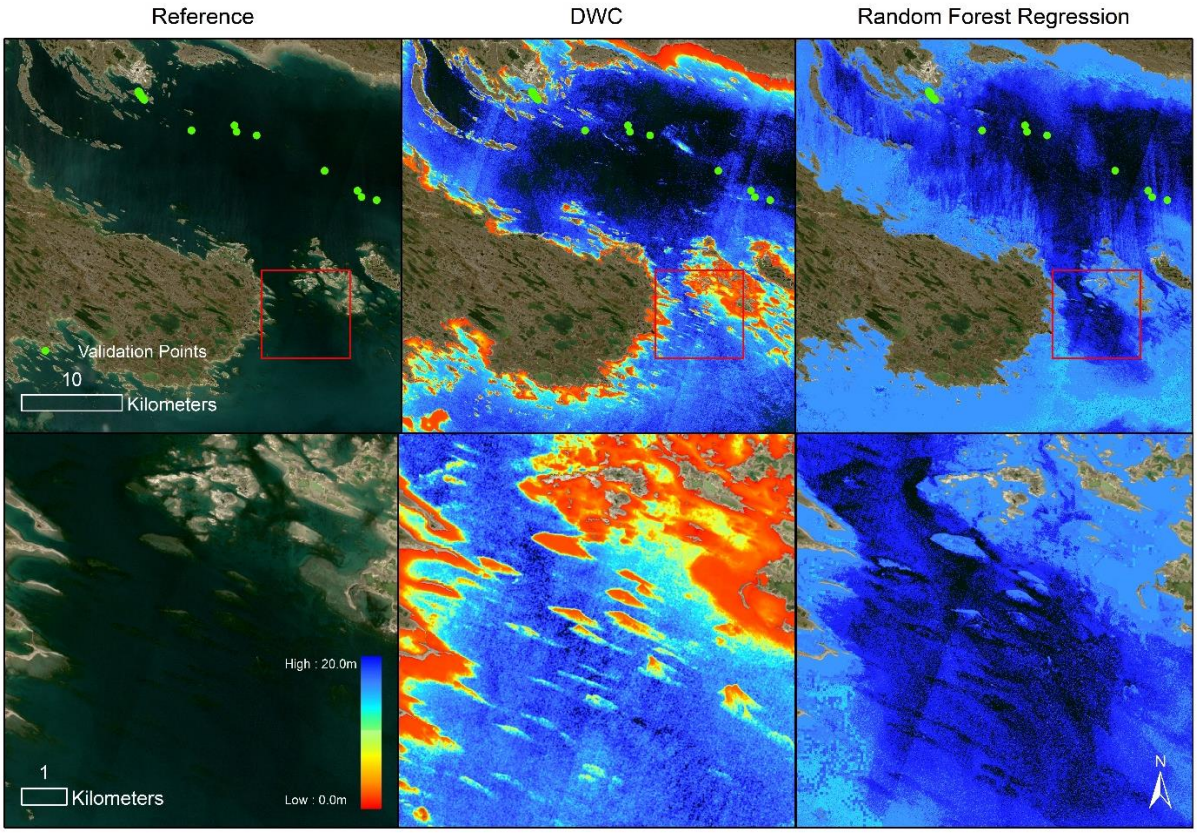

Figure 13 – Rankin Inlet SDB using DWC and RFR. RFR is unable to make predictions in shallow water as there are no calibration data points shallower than 10 m, whereas DWC does not suffer from this problem.

Chapter 3

Conclusion

This study compared the possibility of using the most common SDB methods in use by hydrographic organizations, across seven sites in the Canadian Arctic, to test their potential for cheap, quick and widespread mapping of water depth in the Canadian Arctic. These sites have differing physical characteristics, and different availability of acoustic and airborne lidar data for SDB calibration and validation, greatly impacting the suitability for each site for SDB analysis. The study demonstrated that, of the SDB methods tested here, Random Forest Regression is the best option for predicting bathymetry when a large high-quality calibration dataset is available, whereas the Ratio Transform Algorithm and Multiband methods had worse performance across sites, imagery, and depth ranges. In comparison to these three empirical methods, physics-based SDB, based on the ALUT method and atmospheric correction with either the ACOLITE or Deep Water Correction methods, had relatively higher errors. Nevertheless, in areas where no or poor depth data exist, visual assessment suggests that physics-based SDB produces reasonable results, and at the very least can be used to identify shallow bathymetry features in unsurveyed areas. Given that only a small fraction of the Canadian Arctic is surveyed to modern standards, physics-based SDB is often the only available option. Even with relatively large errors, bathymetric information derived from physics-based SDB can serve to inform decisions about shipping lanes and to reduce risk to vessels traveling in poorly charted areas.

References

Anisimov, O. A., Vaughan, D. G., Callaghan, T., Furgal, C., Marchant, H., Prowse, T. D., … Walsh, J. E. (2007). Polar regions (Arctic and Antarctic). *Climate Change 2007: Impacts, Adaptation and Vulnerability. Contribution OfWorking Group II to the Fourth As- Sessment Report of the Intergovernmental Panel on Climate Change*, 653–685.

Breiman, L. (2001). Random forests. *Machine Learning*, (45), 5–32. https://doi.org/10.1201/9780367816377-11

Casal, G., Hedley, J. D., Monteys, X., Harris, P., Cahalane, C., & McCarthy, T. (2020). Satellite-derived bathymetry in optically complex waters using a model inversion approach and Sentinel-2 data. *Estuarine, Coastal and Shelf Science*, *241*(March), 106814. https://doi.org/10.1016/j.ecss.2020.106814

Chénier, R., Ahola, R., Sagram, M., Faucher, M. A., & Shelat, Y. (2019). Consideration of level of confidence within multi-approach satellite-derived bathymetry. *ISPRS International Journal of Geo-Information*, *8*(1). https://doi.org/10.3390/ijgi8010048

Chénier, R., Faucher, M. A., & Ahola, R. (2018). Satellite-derived bathymetry for improving Canadian Hydrographic Service charts. *ISPRS International Journal of Geo-Information*, *7*(8). https://doi.org/10.3390/ijgi7080306

Hedley, J. (2018). *Atmospheric correction of Sentinel-2 and Landsat 8 for satellite derived bathymetry*. 8.

Hedley, J. D., Harborne, A. R., & Mumby, P. J. (2005). Simple and robust removal of sun glint for mapping shallow-water benthos. *International Journal of Remote Sensing*, *26*(10), 2107–2112. https://doi.org/10.1080/01431160500034086

Hedley, J., Roelfsema, C., & Phinn, S. R. (2009). Efficient radiative transfer model inversion for remote sensing applications. *Remote Sensing of Environment*. https://doi.org/10.1016/j.rse.2009.07.008

Hodúl, M., Chénier, R., Faucher, M. A., Ahola, R., Knudby, A., & Bird, S. (2020). Photogrammetric Bathymetry for the Canadian Arctic. In *Marine Geodesy* (Vol. 43). https://doi.org/10.1080/01490419.2019.1685030

IHO. (2018). INTERNATIONAL HYDROGRAPHIC ORGANIZATION REGULATIONS OF THE IHO FOR INTERNATIONAL (INT) CHARTS and. *The International Hydrographic Bureau Monaco, Edition 4.*(September), 1–435. Retrieved from https://www.iho.int/iho_pubs/standard/S-4/S-4_e4.4.0_EN_Sep13.pdf

Knudby, A., Ahmad, S. K., & Ilori, C. (2016). The Potential for Landsat-Based Bathymetry in Canada. *Canadian Journal of Remote Sensing*, *42*(4), 367–378. https://doi.org/10.1080/07038992.2016.1177452

Labsphere. (2011). *Reflectance Materials and Coatings*. 26. Retrieved from

http://www.labsphere.com

Leach, K., Reinhart, J., Kepkay, M., Kooka, K., Miller, M., & Nappert, M.-S. (2014). *2014 Fall Report of the Commissioner of the Environment and Sustainable Development: Chapter 3 - Marine Navigation in the Arctic*. Retrieved from http://www.oag-bvg.gc.ca/internet/English/att__e_39878.html

Lee, Z., Carder, K. L., Mobley, C. D., Steward, R. G., & Patch, J. S. (1998). Hyperspectral remote sensing for shallow waters I A semianalytical model. *Applied Optics*, *37*(27), 6329. https://doi.org/10.1364/ao.37.006329

Lee, Z., Carder, K. L., Mobley, C. D., Steward, R. G., & Patch, J. S. (1999). Hyperspectral remote sensing for shallow waters: 2 Deriving bottom depths and water properties by optimization. *Applied Optics*, *38*(18), 3831. https://doi.org/10.1364/ao.38.003831

Lyzenga, D. R. (1978). Passive remote sensing techniques for mapping water depth and bottom features. *Applied Optics*, *17*(3), 379. https://doi.org/10.1364/ao.17.000379

Lyzenga, D. R. (1985). Shallow-water bathymetry using combined lidar and passive multispectral scanner data. *International Journal of Remote Sensing*, *6*(1), 115–125. https://doi.org/10.1080/01431168508948428

Maritorena, S., Morel, A., & Gentili, B. (1994). Diffuse reflectance of oceanic shallow waters: Influence of water depth and bottom albedo. *Limnology and Oceanography*, *39*(7), 1689–1703. https://doi.org/10.4319/lo.1994.39.7.1689

Mobley, C. D., Sundman, L. K., Davis, C. O., Bowles, J. H., Downes, V., Leathers, R. A., … Gleason, A. (2005). Interpretation of hyperspectral remote-sensing imagery by spectrum matching and look-up tables. *Applied Optics*, *44*(17), 3576–3592.

Newman, C. M., & LeDrew, E. F. (2001). Assessment of beer's law of logarithmic attenuation for remote sensing of shallow tropical waters. *International Geoscience and Remote Sensing Symposium (IGARSS)*, *3*(C), 1539–1541. https://doi.org/10.1109/igarss.2001.976904

Oceans North Conservation Society, WWF-Canada, & Ducks Unlimited Canada. (2018). *Canada's Arctic Marine Atlas*. Retrieved from https://oceansnorth.org/wp-content/uploads/2018/09/Canadas-Arctic-Marine-Atlas.pdf

Pahlevan, N., Schott, J. R., Franz, B. A., Zibordi, G., Markham, B., Bailey, S., … Strait, C. M. (2017). Landsat 8 remote sensing reflectance (Rrs) products: Evaluations, intercomparisons, and enhancements. *Remote Sensing of Environment*. https://doi.org/10.1016/j.rse.2016.12.030

Parrish, C. E., Magruder, L. A., Neuenschwander, A. L., Forfinski-Sarkozi, N., Alonzo, M., & Jasinski, M. (2019). Validation of ICESat-2 ATLAS bathymetry and analysis of ATLAS's bathymetric mapping performance. *Remote Sensing*, *11*(14). https://doi.org/10.3390/rs11141634

Petit, T., Bajjouk, T., Mouquet, P., Rochette, S., Vozel, B., & Delacourt, C. (2017). Hyperspectral remote sensing of coral reefs by semi-analytical model inversion – Comparison of different inversion setups. *Remote Sensing of Environment*, *190*, 348–365. https://doi.org/10.1016/j.rse.2017.01.004

Philpot, W. D. (1989). Bathymetric mapping with passive multispectral imagery. *Applied Optics*, *28*(8), 1569–1578.

Poupardin, A., Idier, D., De Michele, M., & Raucoules, D. (2016). Water Depth Inversion from a Single SPOT-5 Dataset. *IEEE Transactions on Geoscience and Remote Sensing*, *54*(4), 2329–2342. https://doi.org/10.1109/TGRS.2015.2499379

QGIS.org. (2017). *QGIS Geographic Information System*. Retrieved from http://qgis.org

Stumpf, R. P., Holderied, K., & Sinclair, M. (2003). Determination of water depth with high-resolution satellite imagery over variable bottom types. *Limnol. Oceanogr*, *48*(2), 547–556.

Vanhellemont, Q. (2019). Adaptation of the dark spectrum fitting atmospheric correction for aquatic applications of the Landsat and Sentinel-2 archives. *Remote Sensing of Environment*, *225*(October 2018), 175–192. https://doi.org/10.1016/j.rse.2019.03.010

Vanhellemont, Q., & Ruddick, K. (2014). Turbid wakes associated with offshore wind turbines observed with Landsat 8. *Remote Sensing of Environment*. https://doi.org/10.1016/j.rse.2014.01.009

Vanhellemont, Q., & Ruddick, K. (2015). Advantages of high quality SWIR bands for ocean colour processing: Examples from Landsat-8. *Remote Sensing of Environment*. https://doi.org/10.1016/j.rse.2015.02.007

Vanhellemont, Q., & Ruddick, K. (2016). Acolite for Sentinel-2 : Aquatic Applications of Msi Imagery. *2016 ESA Living Planet Symposium*, (May), 9–13.

Vanhellemont, Q., & Ruddick, K. (2018). Atmospheric correction of metre-scale optical satellite data for inland and coastal water applications. *Remote Sensing of Environment*, *216*(March), 586–597. https://doi.org/10.1016/j.rse.2018.07.015

Appendix A

Scatter Plots

Landsat 8 Results

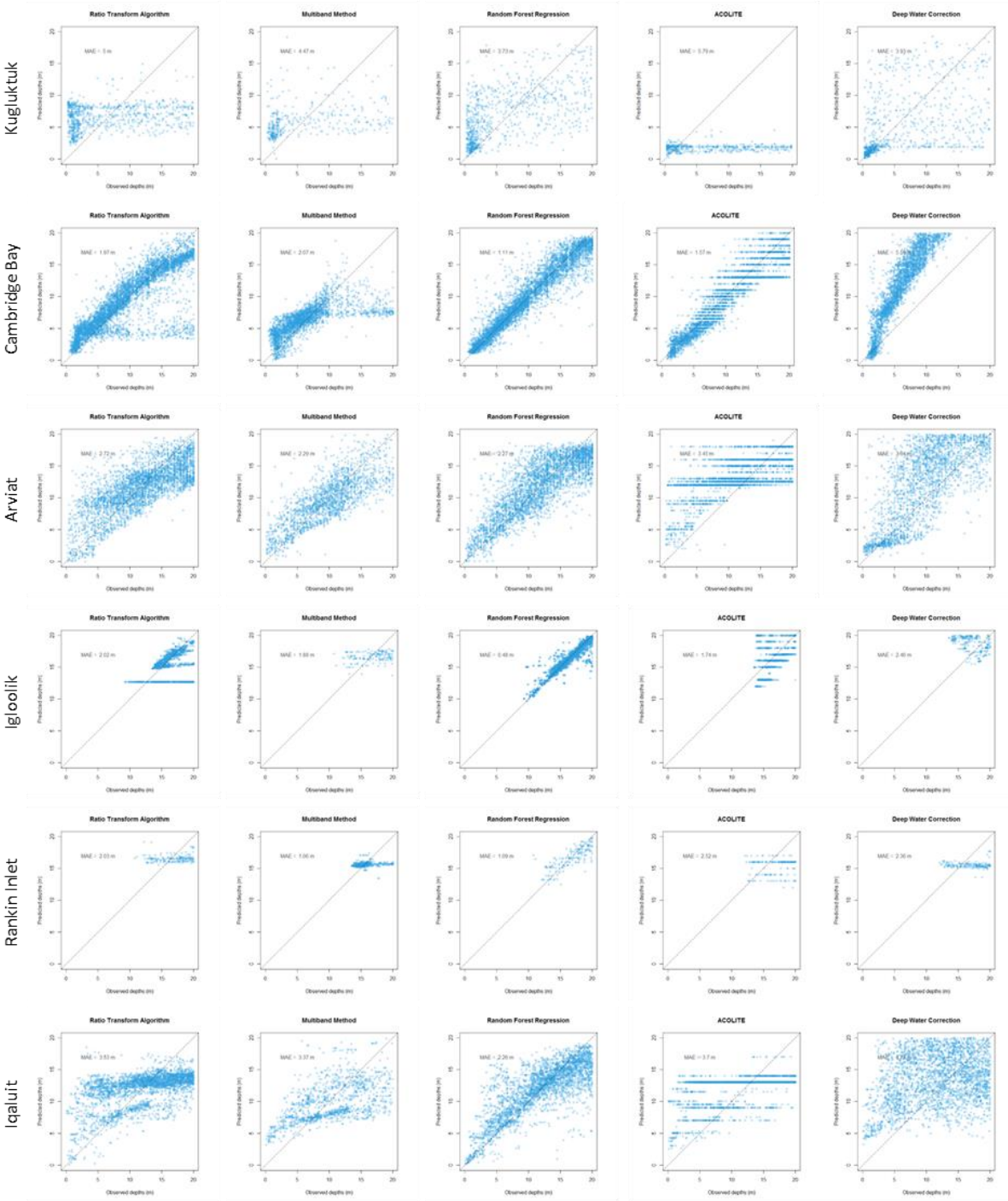

Sentinel-2 Results

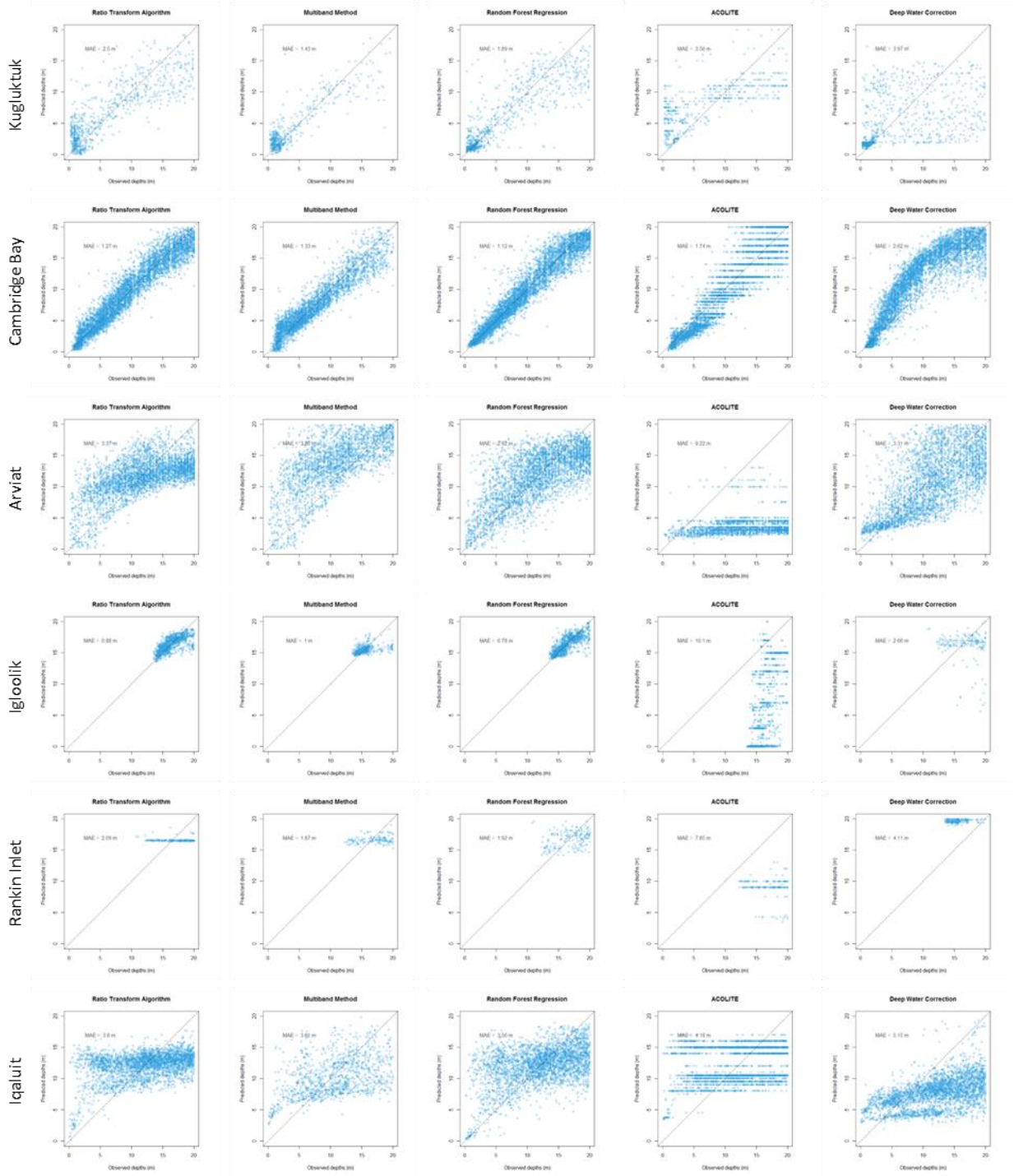

Statistical Analysis Results

1 Kugluktuk

1.1 Landsat 8

Depth Intervals	Ratio Transform Algorithm		Multiband Method		Random Forest Regression		ACOLITE		Deep Water Correction	
(m)	Bias	MAE	Bias	MAE	Bias	MAE	Bias	MAE	Bias	MAE
0 – 20	0.29	5.00	0.00	4.47	0.45	3.73	-5.23	5.79	-1.06	3.93
0 – 2	NA	NA	-0.54	0.92	0.07	0.72	-5.45	5.92	-1.49	1.93
2 – 4	0.82	2.60	1.63	2.46	0.30	2.22	-4.14	5.20	-3.56	4.23
4 – 6	-0.77	4.75	-1.01	4.99	-0.30	4.54	-5.14	5.14	-5.05	6.57
6 – 8	0.21	5.29	-0.73	4.76	-0.36	5.50	NA	NA	-0.86	5.14
8 – 10	1.13	5.88	-1.15	5.67	0.55	4.32	NA	NA	-1.02	4.96
10 – 12	2.58	3.89	4.36	4.91	1.96	5.15	NA	NA	3.49	5.98
12 – 14	0.32	4.59	2.90	6.01	0.19	4.44	NA	NA	3.47	5.10
14 – 16	2.97	2.97	4.48	6.51	3.00	5.73	NA	NA	4.13	5.88
16 – 18	NA	NA	NA	NA	1.71	3.40	NA	NA	6.04	6.77
18 – 20	NA	NA	15.8	15.8	3.15	3.15	NA	NA	4.52	4.92

1.2 Sentinel-2

Depth Intervals	Ratio Transform Algorithm		Multiband Method		Random Forest Regression		ACOLITE		Deep Water Correction	
(m)	Bias	MAE	Bias	MAE	Bias	MAE	Bias	MAE	Bias	MAE
0 – 20	0.08	2.50	0.17	1.43	-0.41	1.89	0.90	3.56	-0.97	3.97
0 – 2	-0.51	0.90	-0.17	0.64	-0.30	0.63	0.56	0.57	-0.12	1.19
2 – 4	1.23	1.67	1.03	1.40	0.51	1.12	1.27	1.40	-4.45	5.18
4 – 6	1.91	2.66	0.87	2.09	0.07	1.90	2.52	3.01	-4.71	6.35
6 – 8	1.11	2.67	0.36	1.50	-0.64	2.97	4.99	5.25	-2.96	5.75
8 – 10	-1.59	3.39	-1.94	2.74	-2.02	3.39	0.16	3.79	-0.15	4.75
10 – 12	-1.24	4.19	-0.54	2.42	-1.61	3.92	-1.65	4.05	2.63	6.05
12 – 14	-0.71	3.27	-1.73	3.19	-0.80	3.39	-3.28	3.38	3.21	5.40
14 – 16	-1.05	3.01	-0.38	1.32	0.39	2.88	6.46	8.41	1.80	4.23
16 – 18	1.40	3.15	1.64	3.77	0.42	2.85	0.69	3.11	13.0	13.0
18 – 20	1.84	2.23	0.64	1.59	2.73	2.73	4.72	4.72	NA	NA

2 Cambridge Bay

2.1 Landsat 8

Depth Intervals	Ratio Transform Algorithm		Multiband Method		Random Forest Regression		ACOLITE		Deep Water Correction	
(m)	Bias	MAE	Bias	MAE	Bias	MAE	Bias	MAE	Bias	MAE
0 – 20	-0.14	1.97	-0.06	2.07	-0.01	1.11	-0.60	1.57	5.52	5.59
0 – 2	0.17	0.50	-0.99	1.08	-0.06	0.38	-0.57	0.63	-0.41	0.48
2 – 4	-0.58	2.29	0.79	1.30	-0.01	0.70	-0.20	0.84	0.89	0.94
4 – 6	-0.83	2.98	1.27	1.72	-0.02	0.78	-0.66	1.11	2.56	2.56
6 – 8	0.43	1.71	-0.62	2.46	0.11	1.00	-0.62	1.28	3.93	3.93
8 – 10	0.53	1.55	-1.36	2.43	0.04	1.07	-0.07	1.16	4.54	4.54
10 – 12	0.80	1.76	-1.06	2.47	0.11	1.39	-0.01	1.36	5.54	5.54
12 – 14	0.32	1.52	0.12	2.34	-0.20	1.64	-1.49	2.46	6.53	6.53
14 – 16	-0.60	1.64	2.68	3.38	-0.12	1.61	-1.21	2.36	7.32	7.32
16 – 18	-1.16	2.13	3.97	3.97	-0.10	1.35	-0.16	1.71	8.11	8.11
18 – 20	0.84	1.48	7.79	7.79	0.18	1.05	1.47	1.67	8.79	8.79

2.2 Sentinel-2

Depth Intervals	Ratio Transform Algorithm		Multiband Method		Random Forest Regression		ACOLITE		Deep Water Correction	
(m)	Bias	MAE	Bias	MAE	Bias	MAE	Bias	MAE	Bias	MAE
0 – 20	0.00	1.27	-0.05	1.33	-0.01	1.12	-0.37	1.74	1.90	2.62
0 – 2	-0.43	0.54	-0.60	0.72	-0.11	0.38	-0.75	0.77	-0.37	0.44
2 – 4	-0.01	0.85	0.39	0.93	-0.10	0.69	-1.03	1.31	0.50	0.86
4 – 6	0.06	1.14	0.52	1.23	-0.03	0.79	-1.57	1.70	1.06	1.31
6 – 8	0.10	1.18	0.15	1.24	-0.03	0.98	-0.96	1.52	1.91	2.16
8 – 10	0.37	1.14	-0.31	1.31	0.02	0.99	-0.62	1.45	2.61	3.07
10 – 12	0.48	1.51	-0.70	1.75	0.20	1.39	-0.85	2.03	2.88	3.56
12 – 14	-0.16	1.59	-1.33	2.03	-0.13	1.65	-0.24	2.01	2.55	4.04
14 – 16	-0.39	1.74	-0.46	1.81	-0.06	1.61	-0.52	2.04	2.48	3.45
16 – 18	-0.41	1.55	0.04	1.66	0.02	1.61	0.50	2.10	1.74	2.52
18 – 20	0.51	1.23	1.49	1.74	0.26	1.13	2.28	2.39	1.75	2.06

3 Arviat

3.1 Landsat 8

Depth Intervals	Ratio Transform Algorithm		Multiband Method		Random Forest Regression		ACOLITE		Deep Water Correction	
(m)	Bias	MAE	Bias	MAE	Bias	MAE	Bias	MAE	Bias	MAE
0 – 20	-0.17	2.72	-0.14	2.29	0.05	2.27	1.64	3.45	2.33	3.64
0 – 2	-1.08	1.33	-0.49	1.42	-0.56	1.00	-1.84	1.90	0.02	1.24
2 – 4	-0.41	1.47	0.73	1.17	0.33	1.13	1.15	1.93	-0.69	1.49
4 – 6	0.06	1.90	0.46	1.75	0.23	1.61	2.77	2.77	-1.04	2.28
6 – 8	0.46	2.65	-0.18	2.39	-0.32	1.94	3.56	3.56	-0.03	2.42
8 – 10	1.15	2.71	-0.40	2.27	-0.15	2.05	3.80	3.81	1.30	2.56
10 – 12	-0.14	2.97	-0.61	2.51	-0.05	2.39	4.78	4.91	1.46	3.18
12 – 14	-0.91	3.05	-0.88	2.49	-0.09	2.81	1.20	3.67	2.22	3.86
14 – 16	-0.94	2.81	0.70	2.64	-0.02	2.66	0.68	2.88	3.67	4.34
16 – 18	0.25	2.22	1.76	2.68	0.38	2.28	1.66	2.85	4.43	4.99
18 – 20	1.15	1.96	2.74	2.90	1.39	2.39	1.81	2.68	5.13	5.27

3.2 Sentinel-2

Depth Intervals	Ratio Transform Algorithm		Multiband Method		Random Forest Regression		ACOLITE		Deep Water Correction	
(m)	Bias	MAE	Bias	MAE	Bias	MAE	Bias	MAE	Bias	MAE
0 – 20	-0.16	3.37	3.05	3.86	-0.02	2.92	-9.12	9.22	-0.66	3.31
0 – 2	-1.14	1.42	-1.58	1.69	-0.79	1.28	-3.25	3.56	-0.09	0.91
2 – 4	0.29	1.55	0.17	1.61	-0.31	1.83	-9.44	9.49	0.27	1.47
4 – 6	0.97	1.94	0.72	1.92	-0.55	2.26	-9.30	9.35	-1.94	2.76
6 – 8	1.62	2.61	1.72	2.69	-0.02	2.38	-10.7	10.7	-2.50	3.49
8 – 10	1.61	3.14	3.47	3.85	-0.39	2.87	-3.03	4.28	-2.21	3.61
10 – 12	-0.44	3.38	3.50	3.95	-0.35	3.09	-2.45	3.75	-1.96	3.63
12 – 14	-1.53	3.88	3.51	4.19	-0.26	3.44	-1.25	2.27	-1.26	3.66
14 – 16	0.23	3.36	3.01	4.13	0.30	3.21	NA	NA	0.69	3.50
16 – 18	2.46	3.38	3.11	3.98	0.88	2.75	NA	NA	2.13	3.42
18 – 20	2.38	2.70	3.92	4.15	1.55	1.97	NA	NA	3.83	4.08

4 Rankin Inlet

4.1 Landsat 8

Depth Intervals	Ratio Transform Algorithm		Multiband Method		Random Forest Regression		ACOLITE		Deep Water Correction	
(m)	Bias	MAE	Bias	MAE	Bias	MAE	Bias	MAE	Bias	MAE
0 – 20	-0.21	2.03	-0.06	1.88	-0.10	1.09	-1.53	2.52	-1.35	2.36
0 – 2	NA	NA	NA	NA	NA	NA	NA	NA	NA	NA
2 – 4	NA	NA	NA	NA	NA	NA	NA	NA	NA	NA
4 – 6	NA	NA	NA	NA	NA	NA	NA	NA	NA	NA
6 – 8	NA	NA	NA	NA	NA	NA	NA	NA	NA	NA
8 – 10	NA	NA	NA	NA	NA	NA	NA	NA	NA	NA
10 – 12	NA	NA	NA	NA	NA	NA	-6.90	6.90	NA	NA
12 – 14	NA	NA	-2.21	2.70	-0.09	0.79	-3.31	3.39	-4.61	4.61
14 – 16	0.83	1.89	0.16	1.96	0.26	1.40	-1.26	2.26	-1.46	2.32
16 – 18	-0.37	2.01	-0.05	1.85	-0.29	1.23	-0.31	2.40	0.33	2.42
18 – 20	0.72	2.89	NA	NA	-0.15	0.68	NA	NA	NA	NA

4.2 Sentinel-2

Depth Intervals	Ratio Transform Algorithm		Multiband Method		Random Forest Regression		ACOLITE		Deep Water Correction	
(m)	Bias	MAE	Bias	MAE	Bias	MAE	Bias	MAE	Bias	MAE
0 – 20	-0.16	2.09	-0.27	1.87	0.00	1.92	-7.85	7.85	-0.66	2.66
0 – 2	NA	NA	NA	NA	NA	NA	NA	NA	NA	NA
2 – 4	NA	NA	NA	NA	NA	NA	-15.3	15.3	NA	NA
4 – 6	NA	NA	NA	NA	NA	NA	-13.3	13.3	-13.6	13.6
6 – 8	NA	NA	NA	NA	NA	NA	-11.0	11.0	-10.5	10.5
8 – 10	NA	NA	NA	NA	NA	NA	-7.32	7.32	-9.94	9.94
10 – 12	NA	NA	NA	NA	NA	NA	-4.97	4.97	-8.52	8.52
12 – 14	NA	NA	NA	NA	NA	NA	-6.61	6.61	-3.83	3.83
14 – 16	NA	NA	-0.78	2.51	-0.52	2.09	NA	NA	-2.07	3.09
16 – 18	-0.18	2.09	-0.23	1.79	-0.18	1.78	NA	NA	0.38	1.84
18 – 20	2.40	2.40	0.42	1.68	1.46	2.03	NA	NA	1.64	2.41

5 Igloolik

5.1 Landsat 8

Depth Intervals	Ratio Transform Algorithm		Multiband Method		Random Forest Regression		ACOLITE		Deep Water Correction	
(m)	Bias	MAE	Bias	MAE	Bias	MAE	Bias	MAE	Bias	MAE
0 – 20	-1.46	2.02	0.02	1.06	-0.02	0.48	-0.26	1.74	1.43	2.46
0 – 2	NA	NA	NA	NA	NA	NA	NA	NA	NA	NA
2 – 4	NA	NA	NA	NA	NA	NA	NA	NA	NA	NA
4 – 6	NA	NA	NA	NA	NA	NA	NA	NA	NA	NA
6 – 8	NA	NA	NA	NA	NA	NA	NA	NA	NA	NA
8 – 10	NA	NA	NA	NA	-0.08	0.08	NA	NA	NA	NA
10 – 12	NA	NA	NA	NA	0.17	0.29	-2.23	2.23	NA	NA
12 – 14	-3.03	3.29	-4.27	4.27	0.03	0.51	-2.15	2.15	NA	NA
14 – 16	-0.16	1.10	-0.01	1.06	0.06	0.48	-0.81	1.03	-2.03	2.03
16 – 18	0.10	0.66	0.64	0.88	-0.08	0.57	-0.39	1.28	-0.70	1.51
18 – 20	-0.11	0.75	NA	NA	-0.14	0.36	2.44	2.81	2.42	2.83

5.2 Sentinel-2

Depth Intervals	Ratio Transform Algorithm		Multiband Method		Random Forest Regression		ACOLITE		Deep Water Correction	
(m)	Bias	MAE	Bias	MAE	Bias	MAE	Bias	MAE	Bias	MAE
0 – 20	-0.06	0.88	-0.07	1.00	-0.03	0.78	-10.0	10.1	4.10	4.11
0 – 2	NA	NA	NA	NA	NA	NA	-15.3	15.3	NA	NA
2 – 4	NA	NA	NA	NA	NA	NA	-12.9	12.9	NA	NA
4 – 6	NA	NA	NA	NA	NA	NA	-10.8	10.8	NA	NA
6 – 8	NA	NA	NA	NA	NA	NA	-10.0	10.0	NA	NA
8 – 10	NA	NA	NA	NA	NA	NA	-8.05	8.05	NA	NA
10 – 12	NA	NA	NA	NA	NA	NA	-5.42	5.42	NA	NA
12 – 14	-0.33	0.39	NA	NA	-0.02	0.02	-4.78	4.78	NA	NA
14 – 16	-0.16	0.85	-0.12	0.91	-0.10	0.70	-3.26	3.28	NA	NA
16 – 18	0.03	0.92	0.10	1.35	-0.03	0.86	0.67	0.97	NA	NA
18 – 20	-0.15	0.74	0.58	1.22	0.17	0.80	3.25	3.25	4.10	4.11

6 Iqaluit

6.1 Landsat 8

Depth Intervals	Ratio Transform Algorithm		Multiband Method		Random Forest Regression		ACOLITE		Deep Water Correction	
(m)	Bias	MAE	Bias	MAE	Bias	MAE	Bias	MAE	Bias	MAE
0 – 20	0.01	3.53	-0.50	3.37	-0.02	2.26	0.56	3.70	1.78	4.77
0 – 2	-0.85	1.26	NA	NA	-0.55	0.89	NA	NA	NA	NA
2 – 4	0.95	2.02	2.84	2.84	-0.42	1.35	2.21	2.31	3.16	3.16
4 – 6	1.31	2.34	2.79	3.09	-0.18	2.35	2.01	2.67	1.18	4.29
6 – 8	-0.21	2.57	-0.38	2.60	0.59	1.80	0.15	2.79	-1.89	4.97
8 – 10	-1.14	3.71	-2.28	4.13	0.20	2.23	0.69	3.65	-0.36	4.42
10 – 12	1.96	4.67	-0.38	3.77	-0.10	2.56	5.47	6.33	-0.45	4.71
12 – 14	0.01	3.54	-0.89	2.77	-0.19	2.58	0.30	3.68	0.27	4.20
14 – 16	-1.39	3.00	1.02	3.28	0.05	2.56	10.18	10.18	1.59	3.87
16 – 18	1.48	3.25	3.25	4.15	-0.20	1.76	1.88	2.64	4.69	5.25
18 – 20	15.3	15.3	5.50	5.56	0.41	1.13	NA	NA	6.14	6.22

6.2 Sentinel-2

Depth Intervals	Ratio Transform Algorithm		Multiband Method		Random Forest Regression		ACOLITE		Deep Water Correction	
(m)	Bias	MAE	Bias	MAE	Bias	MAE	Bias	MAE	Bias	MAE
0 – 20	0.06	3.80	-0.38	3.61	0.05	3.56	0.46	4.18	-4.33	5.15
0 – 2	0.87	0.91	NA	NA	-0.35	0.68	NA	NA	-1.83	1.83
2 – 4	1.77	2.00	3.15	3.15	-0.50	2.06	3.16	3.16	-3.88	4.71
4 – 6	2.39	2.61	2.93	3.48	-0.85	2.40	2.60	3.14	-4.38	5.52
6 – 8	1.92	2.98	-1.03	2.99	-0.29	3.06	4.40	4.53	-3.63	4.89
8 – 10	-0.80	3.41	-2.15	4.09	-1.45	4.03	-2.11	4.20	-4.95	5.26
10 – 12	-0.50	3.89	-0.43	3.74	-0.74	3.87	-1.53	3.85	-5.37	5.56
12 – 14	0.29	3.97	0.12	3.20	0.52	3.62	0.51	4.16	-4.02	4.54
14 – 16	0.35	3.58	2.28	3.86	1.14	3.67	2.65	4.39	-2.27	2.99
16 – 18	1.85	3.84	3.38	4.07	0.60	2.30	2.85	4.58	1.74	2.95
18 – 20	NA	NA	4.67	4.67	1.48	2.37	NA	NA	0.96	1.95

Appendix B

SDB Tools User Guide

In order to make analysis accessible to communities with limited resources, a series of plugins were developed for the open source GIS software QGIS (QGIS.org, 2017). Technical requirements include the QGIS software version 2.18 Las Palmas, or other QGIS versions that use Python 2.7.

Empirical Plugin Requirements

A single, cloud- and ice-free satellite image with minimal sunglint and a shapefile containing calibration depths in the same region of interest are the only two input requirements for the empirical plugin. Please note, the shapefile MUST be clipped to the image extent for the plugin to work, and the user must know the field name under which the depth data is located as a required input. The plugin will automatically perform a transformation of datum and projection if the spatial references for the two input files are different.

From this map, the user can export contours into the format of their choosing, so long as it is compatible with QGIS.

Physics-based Plugin Requirements

Plugin requirements begin with the user creating a multiband image file from the satellite image, as well as a shapefile of the Region of Interest (ROI), and using a set of seafloor reflectance spectra for the area of interest. The user will be required to run their own atmospheric correction model after deglinting such as ACOLITE, or SeaDAS if using Linux (both will work with Landsat 8 and Sentinel-2 data). DWC uses an at-cost software and is not included with the SDB Tools plugin.

Step-by-Step Instructions

Empirical SDB

The steps followed within the framework of the empirical QGIS plugin are:

1. Select the sensor and method you wish to use for analysis (Figure 14). Click “Next”.

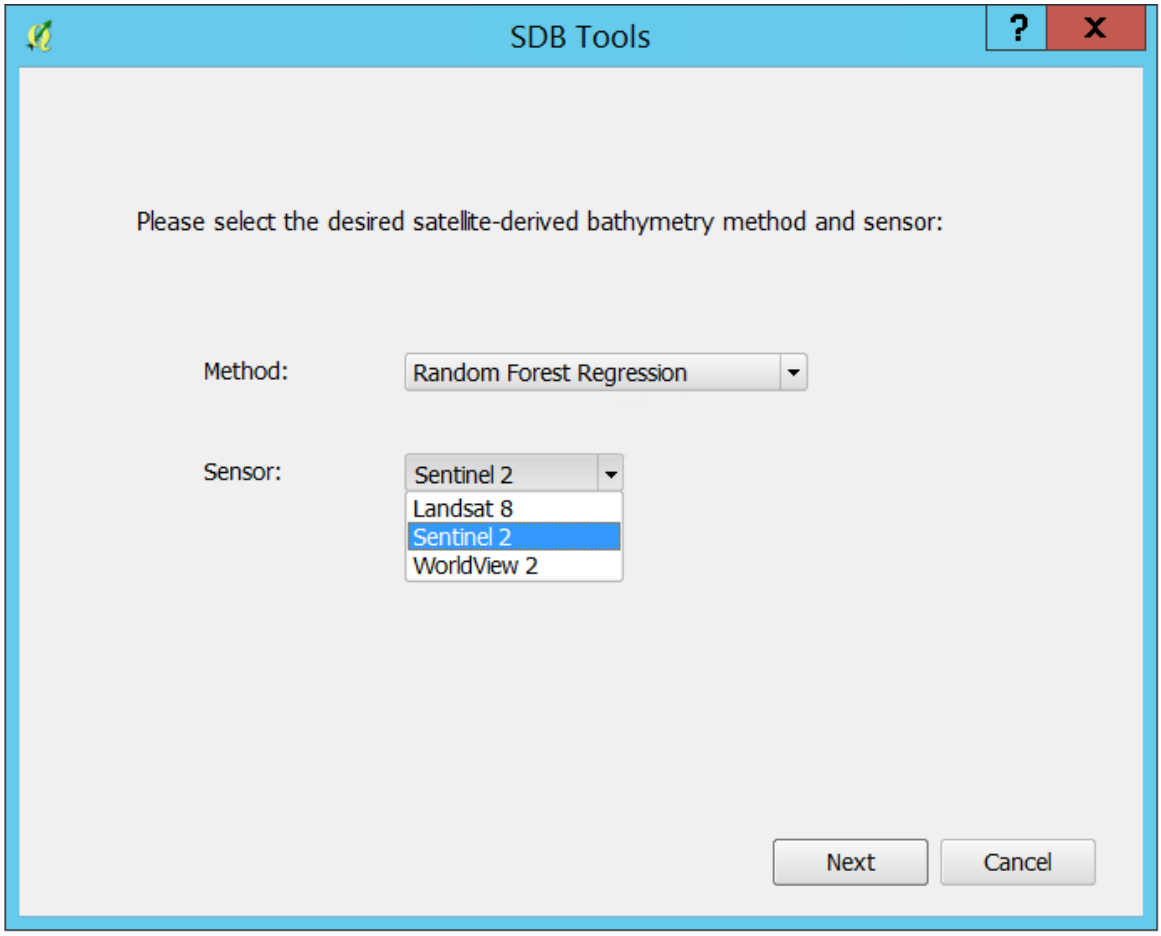

Figure 14 – Start page for the SDB Tools plugin. Select method and sensor here.

2. Select correct metadata and shapefile containing depth data, enter the field in which depth data is stored (Figure 15):

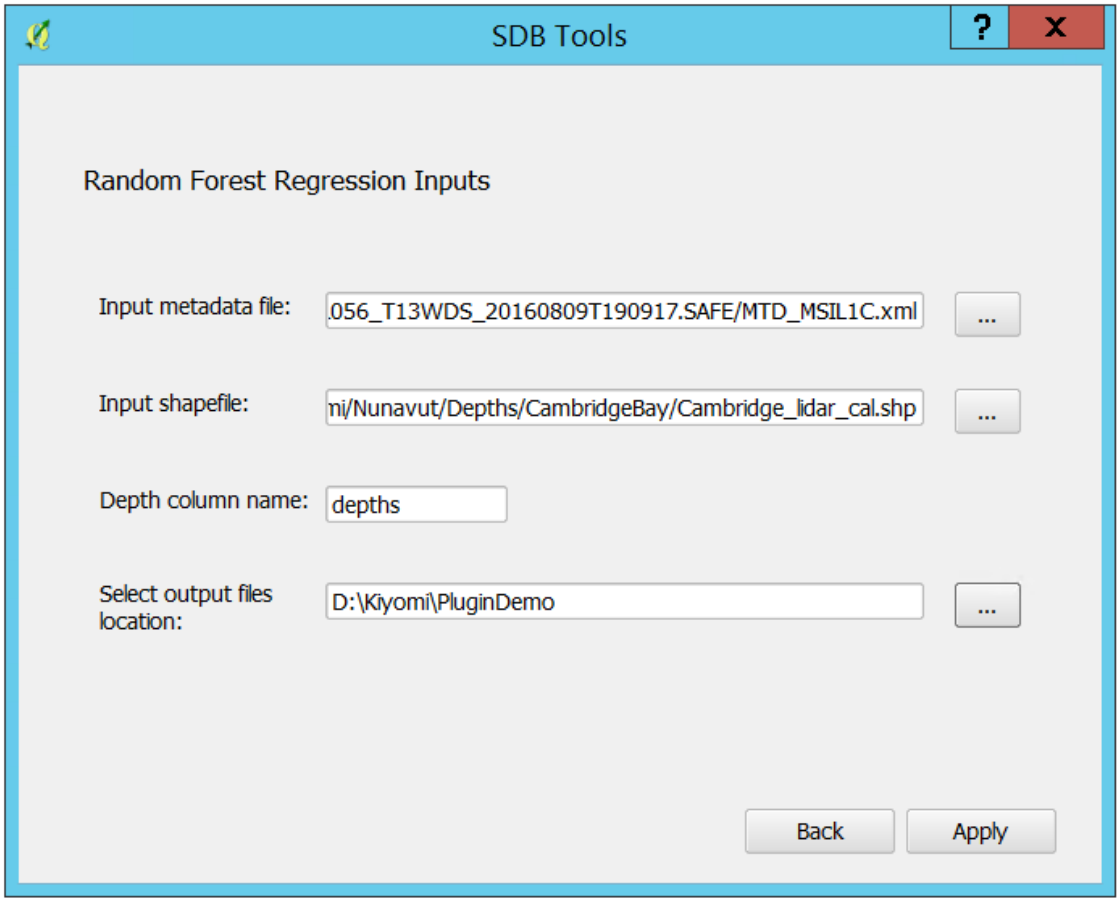

Figure 15 – Browse to the desired inputs. Ensure that the metadata files are the .txt file for Landsat 8 and the .xml file for Sentinel-2 and WorldView-2. Double check that the shapefile is fully within the extent of the satellite image file, and what attribute field the depth data is stored.

Click "Apply" to complete the first step of the selected empirical method.

IMPORTANT NOTE: Nothing will appear to happen, *but the plugin is processing*! This may take anywhere from a couple minutes to approximately 10 minutes, depending on the method selected and the user's processing power. The Ratio Transform Algorithm is the quickest to process, followed by Multiband method, then Random Forest Regression.

3. Visually estimate a reasonable threshold depth, and, in the case of the Ratio Transform Algorithm, an appropriate statistical method. Figure 16 below is for Random Forest Regression:

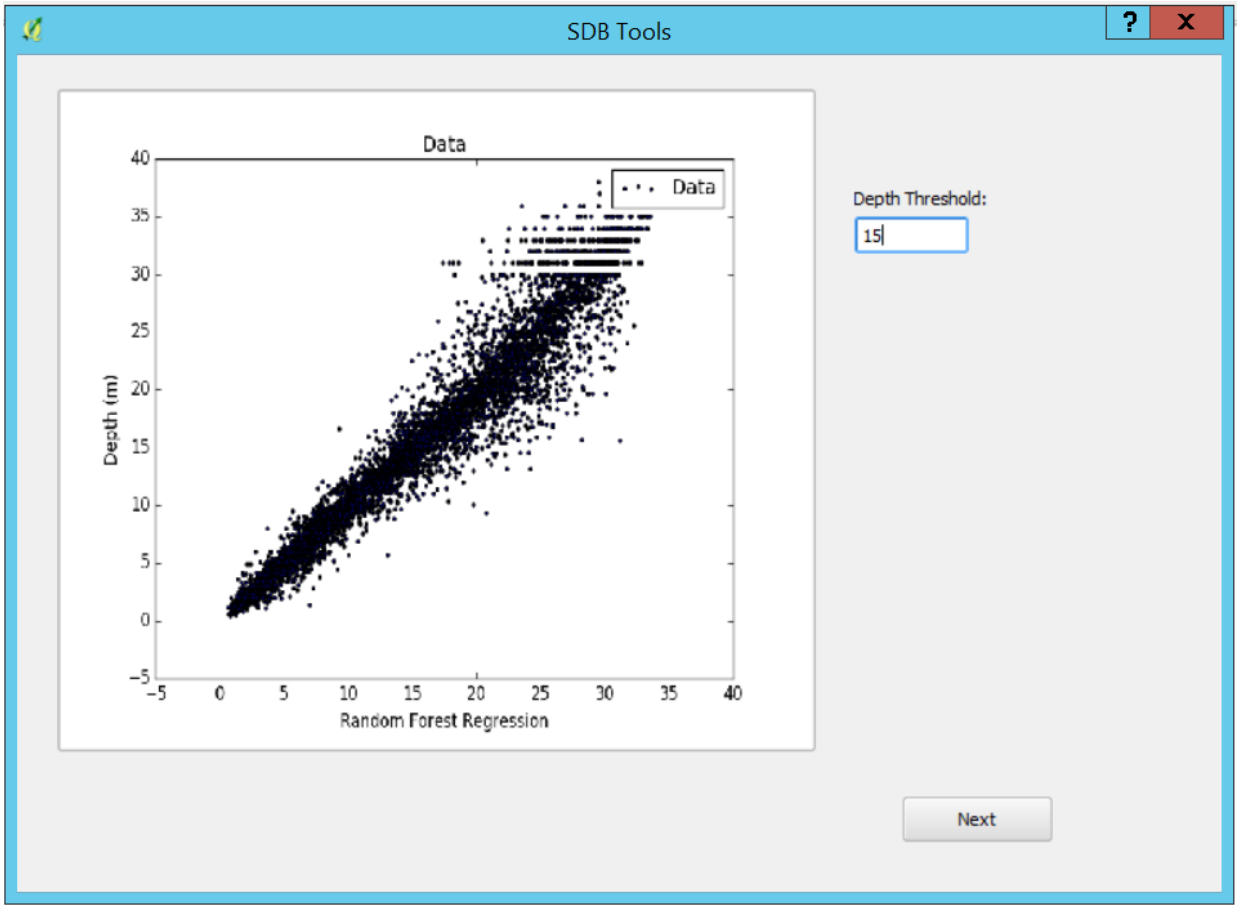

Figure 16 – First plot produced by the plugin with derived depths vs method values. Here the user makes a visual estimate to assign a threshold value beyond which bathymetry estimates are considered poor, and are removed from the image, or in the case of Ratio Transform, the value is used to apply a linear equation to the remainder of the image.

4. The plugin then produces a depth image and two plots: one comparing observed and predicted depths, and the method values against the predicted depths (Figure 17). Your image will be in the default colour ramp of QGIS, as seen in Figure 18.

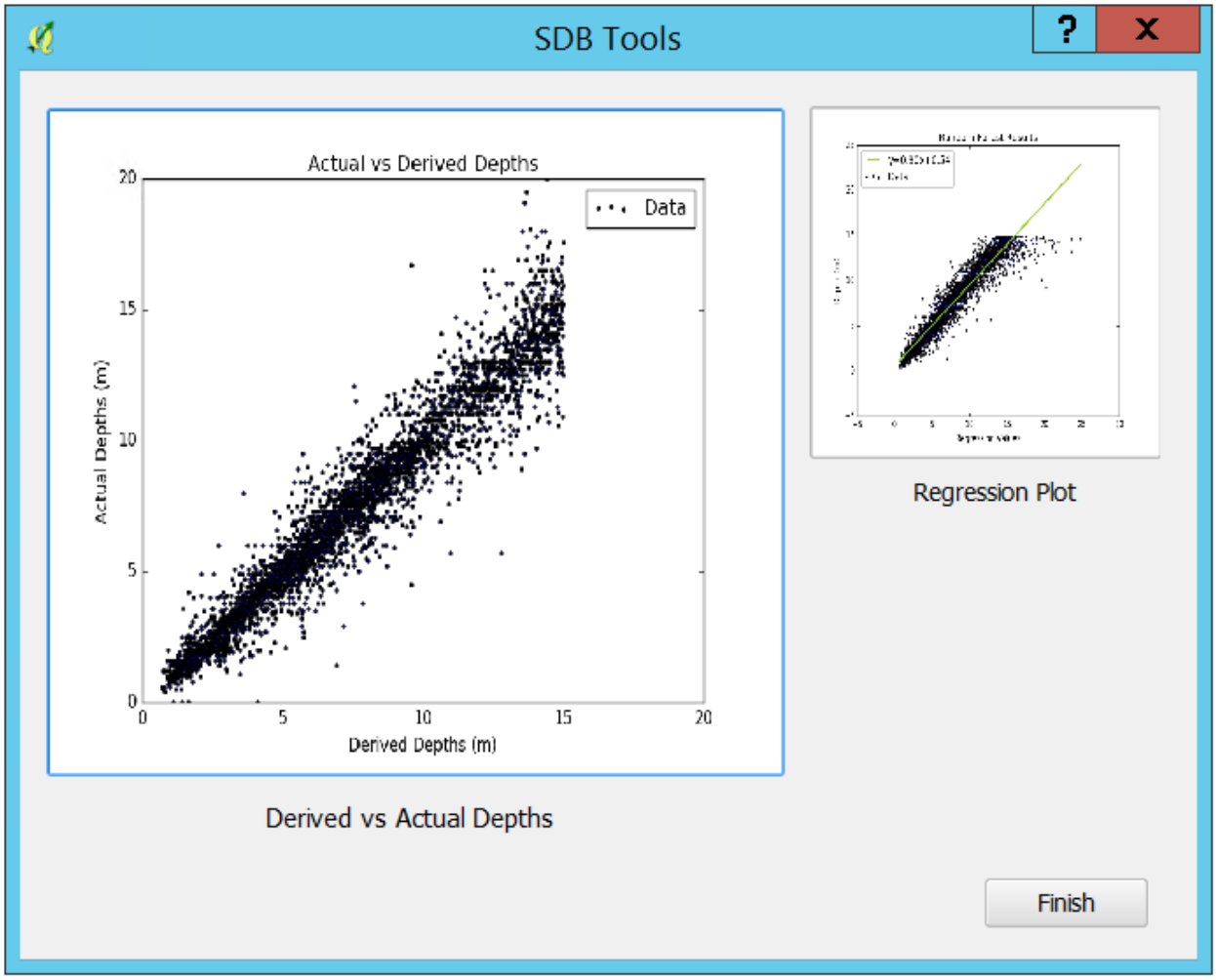

Figure 17 – Final plots produced by the plugin. The large plot is predicted vs observed depths, while the smaller plot is the same as the initial plot produced, minus the threshold limits, and with a trendline and the line equation added in the legend.

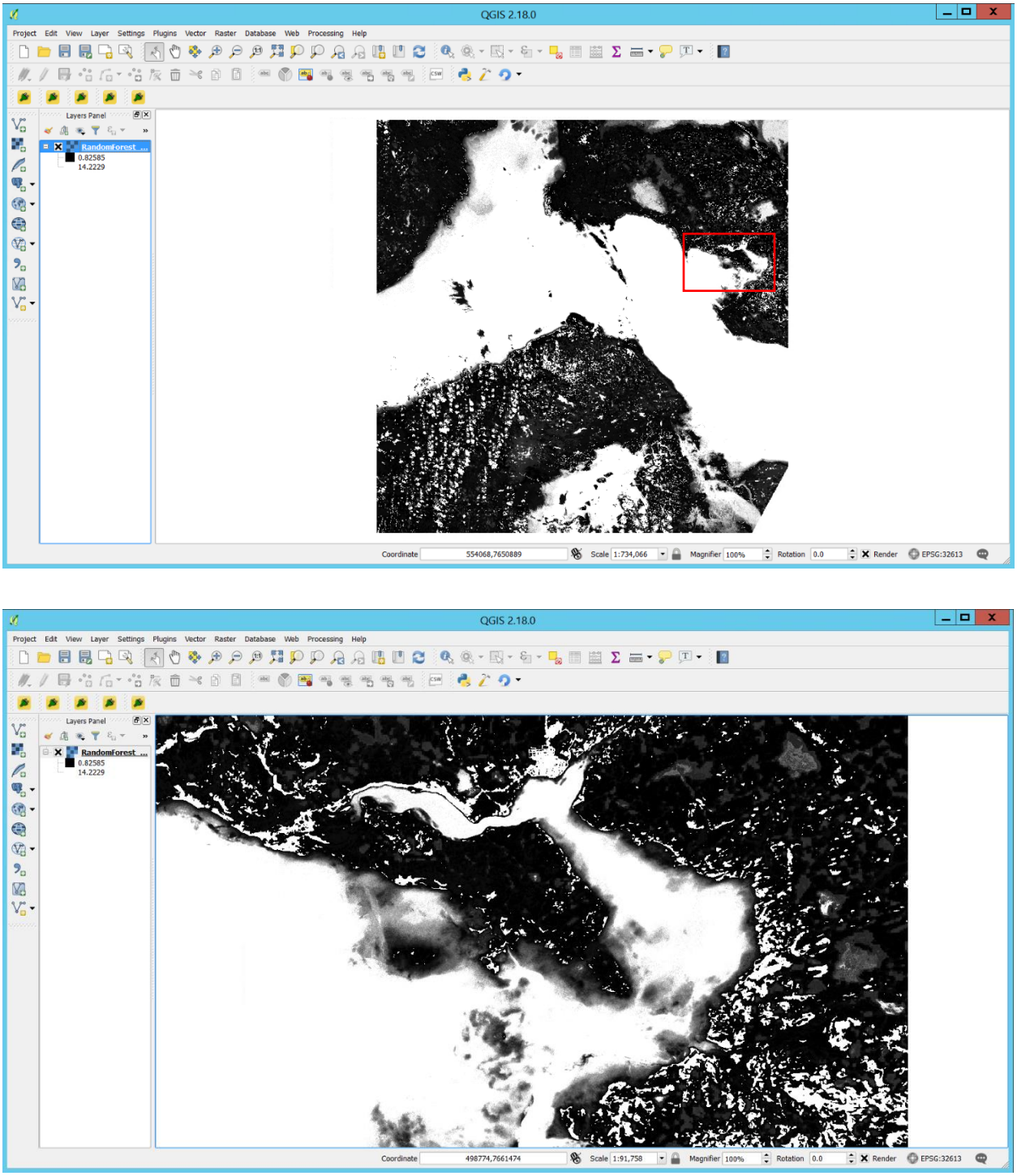

Figure 18 – Image products resulting from the "SDB Tools" plugin. The top image is the entire Sentinel-2 image tile used to assess Cambridge Bay, with the red box indicating the zoomed in at Cambridge Bay itself, seen in the bottom image.

All files produced by the plugin will also be located in the predetermined output folder:

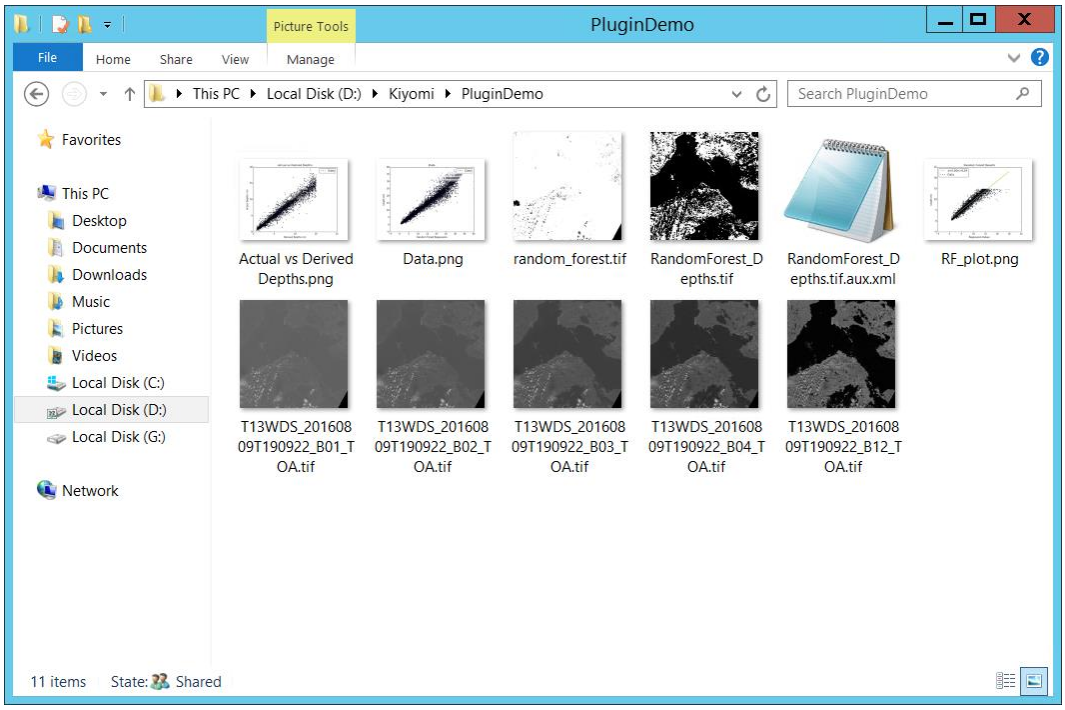

Figure 19 – Folder contents once the plugin has completed processing.

At this time, with the final image product, the user is encouraged to create a land mask as the default values used for the land mask within the plugin are hard-coded and may not always be effective, such as in Figure 18. Additionally, the user can now correct for tidal stage at the time of image capture.

Physics-Based SDB

The steps followed within the framework of the physics-based plugins are:

1. Create a multiband GeoTIFF file. At minimum the file should include bands covering the visible and NIR wavelengths. Bands should be in order of increasing wavelength. Then create a polygon shapefile containing varying levels of sun glint over homogenous deep-water areas in the ROI:

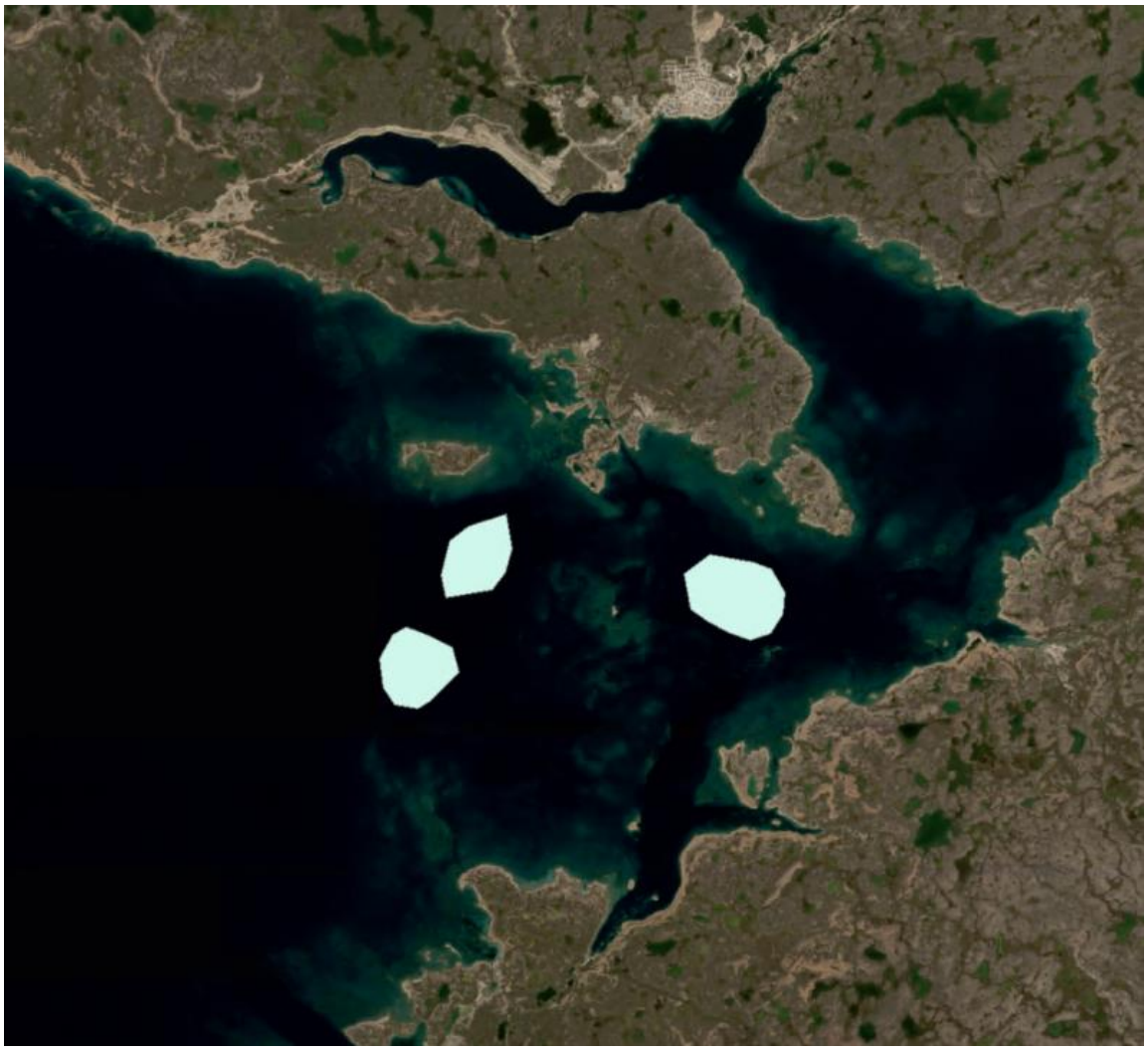

Figure 20 – Initial multispectral GeoTIFF file made with the coastal, blue, green, red, and NIR bands, as well as a shapefile with varying amounts of sun glint.

2. Correct for reflected sunlight of the sea surface in the image with the multiband file using the "Deglint" plugin. To do so, select the newly created multiband file and identify which

band number the NIR band is (be mindful of which number you have assigned this to be), as well as the ROI shapefile and the desired output location and name (Figure 21) to produce your deglinted image (Figure 22).

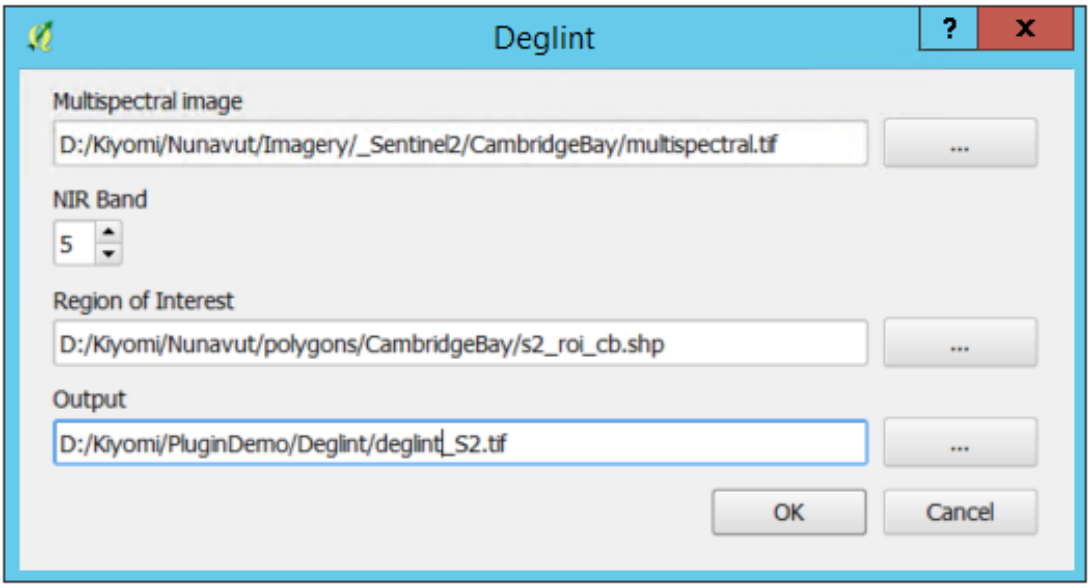

Figure 21 – Deglint inputs for Cambridge Bay.

Figure 22 – Original multispectral file at and area in Cambridge Bay (left) and the newly deglinted file (right). Please note this image was originally selected for its limited sun glint on the sea surface for the empirical methods, and therefore displays a less dramatic difference that might be observed otherwise.

3. Complete atmospheric correction on deglinted image. This currently must be done with an external software.
4. Estimate bathymetry with RTM plugin. You must:
    - Know the solar and view zenith angles (or supply metadata file that contains this information).

- Provide a set of seafloor spectra in a .csv file.
- For our project, we used the following set of parameter specifications, which can be modified by the user (Figure 23):
    - P (Phytoplankton concentrations): 0 – 0.06 mg/m^3
    - G (Gelbstoff): 0 – 0.2 m^{-1}
    - X (Suspended particulate matter concentration): 0 – 0.1 mg/m^3
    - Z (depth): 0 – 30 m

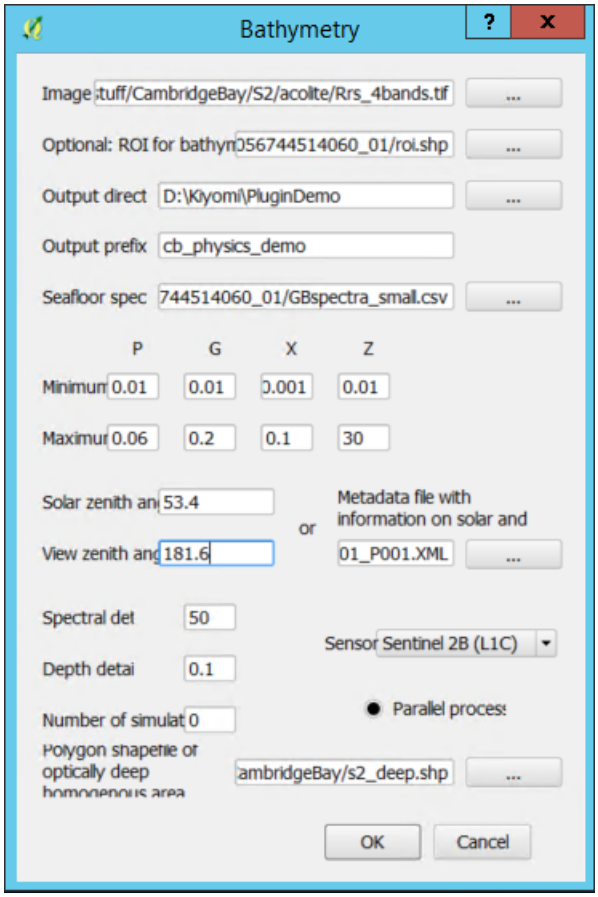

Figure 23 – RTM Bathymetry input GUI example.

- Click “OK” to produce the bathymetry image (Figure 24):

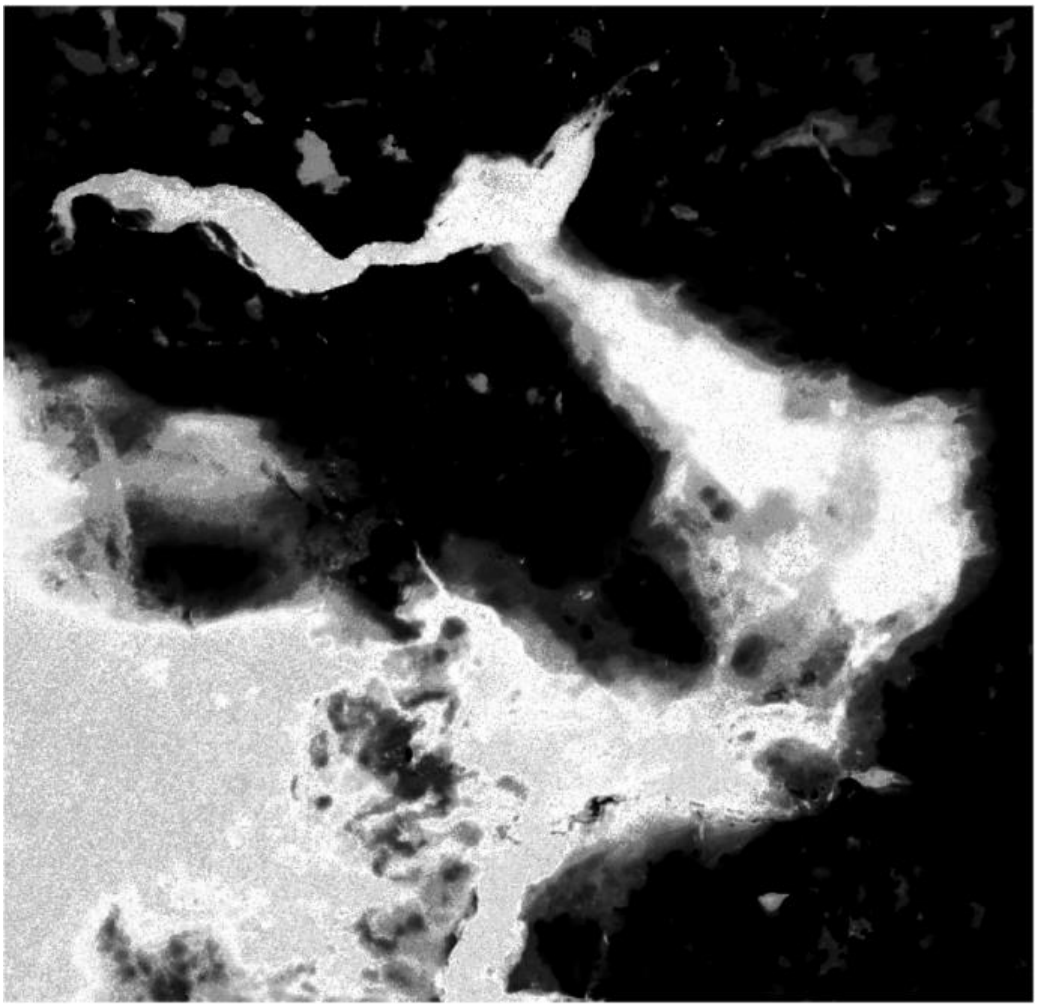

Figure 24 – RTM Bathymetry plugin data product.

Like the Empirical plugin, the user can create a land mask for the bathymetry image produced if desired. The depths from the image are predicted relative to sea level at the time of image acquisition, and would also need to be corrected for tidal stage at the time of image capture.